Macroscopic and microstructural properties of engineered cementitious composites incorporating recycled concrete fines

Li, Junxia; Yang, En-Hua

2017

Li, J., & Yang, E. -H. (2017). Macroscopic and microstructural properties of engineered cementitious composites incorporating recycled concrete fines. Cement and Concrete Composites, 78, 33-42.

https://hdl.handle.net/10356/83180

https://doi.org/10.1016/j.cemconcomp.2016.12.013

Macroscopic and Microstructural Properties of Engineered Cementitious Composites Incorporating Recycled Concrete Fines

Junxia Li[a,b], En-Hua Yang[c,1]

[a]Interdisciplinary Graduate School, Nanyang Technological University, 50 Nanyang Avenue, Singapore 639798

[b]Residues & Resource Reclamation Centre, Nanyang Environment and Water Research Institute, Nanyang Technological University, 1 Cleantech Loop, Singapore 637141

[c]School of Civil and Environmental Engineering, Nanyang Technological University, 50 Nanyang Avenue, Singapore 639798

ABSTRACT

Recycled concrete fines (RCF) are fine aggregates and particles from the demolition waste of old concrete. Unlike recycled coarse aggregates, RCF is seldom used to replace sands in concrete due to its high surface area and attached old mortar on the surface of RCF. This study investigated potential use of RCF as microsilica sand substitute in the production of engineered cementitious composites (ECC), a unique high performance fiber-reinforced cementitious composites featuring extreme tensile strain capacity of several percent. The results showed that it is viable to use RCF as microsilica sand substitute in the production of ECC and the resulting RCF-ECCs possess decent compressive strength and strain capacity. Microstructure investigation on the component level revealed that RCF size and content modify matrix toughness and fiber/matrix interface properties. The influence of RCF size and content on ECC properties was clearly revealed and explained by the resulting fiber bridging $\sigma(\delta)$ curves of RCF-ECCs calculated from the micromechanical model. Micromechanics-

[1] Corresponding author. Tel.: +65 6790 5291; fax: +65 6791 0676. *E-mail address:* ehyang@ntu.edu.sg (E.H. Yang)

based design principle can therefore be used for ingredients selection and component tailoring of RCF-ECCs.

Keywords: Recycled concrete fines; Engineered Cementitious Composites; micromechanical model; single fiber pullout test; wedge splitting test

1. Introduction

The use of construction and demolition waste not only reduces environmental burden by minimizing landfill but also preserves the finite raw materials. Recycled concrete aggregates resulting from the demolition of old concrete structures are available currently in large quantities. Coupled with shortage of non-reactive natural aggregates, there is an urgent need to use the waste aggregates. Many studies have proven that recycled coarse aggregates (RCA) can be an excellent substitution of natural aggregates for concrete production [1-3].

Generally, it is believed that the fine fraction of recycled concrete aggregates, known as recycled concrete fines (RCF), has limited application because of its larger water absorption which can jeopardize the fresh and the hardened properties of concrete. This is attributed to the high surface area and old mortar attached to the fine particles, which creates a weak interface transition zone and prevents proper bonding between the matrix and the fines [4-6].

Investigations on the use of RCF as a partial replacement of natural sand in concrete were carried out to show that the strength at early ages was marginally lower, modulus of elasticity of concrete was reduced by 15% to 20%, and drying shrinkage of concrete was increased by about 40% [7]. A reduction of compressive strength and increased shrinkage also occurred in Khatib's work [8]. Evangelista and Brito [9] reported that the use of RCF, up to 30% replacement, did not have significant influence on the mechanical properties of concrete,

while the modulus of elasticity was reduced with the increase of RCF replacement ratio. The feasibility of utilizing RCF together with recycled coarse aggregate for self-compacting concrete has been demonstrated in [10]. The maximum compressive strength was achieved by using 25%-50% RCF as a replacement of river sand. Yaprak et al. [11] conducted experiments to prove that water absorption of RCF was higher than normal fine aggregate and air content values for the fresh concrete increased. According to the test results obtained, the compressive strength for the hardened concrete decreased.

Engineered cementitious composite (ECC) is a unique class of high performance fiber-reinforced cementitious composite (HPFRCC) developed for structural applications. ECC exhibits tensile strain-hardening behavior with strain capacity in the range of 3-5% [12], whereas the fiber content is 2% by volume or less. The ultra high ductility is achieved by optimizing the microstructure of the composite employing the micromechanics-based model [13]. This approach can take into account the fiber, matrix and interface properties on composite tensile strain-hardening behavior. Based on the design guidance of the micromechanical model, microsilica sand with average and maximum grain sizes of 110 and 200 μm respectively, is widely used. Nevertheless, the availability of microsilica sand is constrained by locality. In this research, RCF is identified as a potential candidate for substitution of microsilica sand in the production of ECC with two goals, one is to achieve high tensile ductility, and the other is to improve the sustainability of the built environment by using waste stream material [14].

2. Design guideline of RCF-ECC

2.1 Micromechanical model

ECC is designed using a well-defined micromechanical model. Desirable composite behavior can be tailored by adjusting the material microstructures. There are two fundamental requirements for strain-hardening behavior. First for all, the steady-state flat crack extension must be prevail under tension, which requires the crack tip toughness J_{tip} to be less than the complementary energy J_b' calculated from the bridging stress σ versus crack opening δ curve, as illustrated by Marshall and Cox [15].

$$J_{tip} \leq \sigma_0 \delta_0 - \int_0^{\delta_0} \sigma(\delta) d\delta = J_b' \quad (1)$$

where $J_{tip}=K_m^2/E_m$, σ_0 is the maximum bridging stress corresponding to the opening δ_0, K_m is the matrix fracture toughness, and E_m is the matrix Young's modulus. The stress-crack opening relationship $\sigma(\delta)$ was derived by using analytic tools of fracture mechanics, micromechanics, and probabilistics. As a result, the $\sigma(\delta)$ curve was expressible as a function of fiber and fiber/matrix interface properties. A numerical process was proposed by Yang et al. [16] to calculate the $\sigma(\delta)$ and to determine J_b'.

Another condition for the strain-hardening behavior is that the matrix first cracking strength σ_{fc} must not exceed the maximum fiber bridging strength σ_B.

$$\sigma_{fc} \leq \sigma_B \quad (2)$$

where σ_{fc} is determined by the matrix fracture K_m, pre-existing internal flaw size a_0, and the $\sigma(\delta)$ curve. Eqn. (1) governs the crack propagation mode, while Eqn. (2) controls the initiation of cracks. Satisfaction of both Eqns. (1) and (2) is necessary to achieve the strain-hardening behavior. Details of micromechanical model can be found in Yang and Li [13].

2.2 Use of RCF

Li et al. [17] presented results of experimental research and theoretical calculations based on micromechanics to investigate the effect of fine aggregate on the strain-hardening behavior of fiber-reinforced cementitious composites. It concluded that the addition of aggregate increases elastic modulus, matrix toughness and matrix tensile strength. A large increase in matrix toughness and matrix tensile strength can lead to a violation of the inequality sign in Eqns. (1) and (2). Therefore, to ensure a robust strain-hardening behavior in the composite, the quantity and the particle size of aggregate used in ECC have to be well selected.

The use of RCF, however, may become an advantage in ECC. The weak bonding between RCF particles and matrix may lead to lower matrix toughness and lower matrix tensile strength, which helps the composite to satisfy Eqns. (1) and (2). For that reason, larger size and higher quantity of RCF might be used to produce ECC with tensile strain-hardening behavior. In addition, the use of RCF is also desirable for economical and environmental considerations due to the substitution of microsilica sand.

3. Experimental program

3.1 Raw materials

Ordinary Portland cement (ASTM C150 Type I) was used in this study. Locally available ground granulated blast-furnace slag (GGBS) was selected as the supplementary cementitious material to partially replace cement with a constant GGBS-to-cement ratio of 0.8. The characteristics of polyvinyl alcohol (PVA) fiber are listed in Table 1. Surface of PVA fibers was coated with hydrophobic oiling agent of 1.2% by weight to control the interface properties of the fiber and matrix and 8mm short fibers were employed in synthesis of RCF-ECC. Polycarboxylate-based comb-polymer superplasticiser, ADVA® 181, was used to control rheological properties of the paste to ensure good fiber dispersion can be achieved.

Recycled concrete fines (RCF) sourced locally in Singapore. To keep the consistent grading of RCF, it was prepared according to modified Fuller's curve [18] and the resulting particle size distributions are shown as Fig. 1. Physical properties of RCF are summarized in Table 2. Due to the high water absorption of RCF, it was processed to attain saturated surface dry (SSD) state by adding water proportionally in advance.

A study of the microstructure of recycled concrete fines (RCF) showed that the particles are irregular and angular in shape and the surface is generally rough and porous. The result is consistent with that of the literature [4]. Compared with the microsilica sand, RCF particles are found to have scattered particle shapes and sizes as shown in Fig. 2, especially a lot of small grains are included in RCF sample. The RCF consists of crushed aggregate particles (Fig. 3) and partially hydrated cement paste which is made up of unhydrated cement grains and hydrated products of cement (Fig. 4).

In Fig. 3, RCF ($d < 300$ μm) showed a distinctive morphology covered by small particles, which contain calcium silicate hydrate, calcium hydroxide usually in the shape of relatively large hexagonal crystals, and ettringite of needle shape [18]. The morphological study of RCF particles reveals that: (1) the high surface area and porosity, which lead to high water absorption; (2) the coating with small particles, which damage the bond between the matrix and RCF and (3) the existence of unhydrated cement grains may contribute to self-cementing property.

3.2 Mix composition of RCF-ECC

According to the micromechanics-based design principles of ECC, RCF content and RCF particle size were identified as important factors governing the properties of RCF-ECC. An experimental program was designed to study the influence of RCF content and particle size on the matrix properties, fiber/matrix interface properties and the resulting RCF-ECC composite mechanical properties as Table 3. The first series is to evaluate the influence of particle size of RCF. The ratio of RCF to cement was fixed at a constant value of 0.2. Four groups of RCF with the maximum particle size of 2,360 μm, 1,180 μm, 600 μm, and 300 μm were used in four mixes, respectively. The second series is to understand the effect of RCF content. The maximum particle size was chosen to be 600 μm, whereas three different dosages of RCF were used in three mixes. All the ratios are by weight except the fiber content is by volume.

3.3 Testing methods

3.3.1 Composite testing

To evaluate composite performance, compressive test and bending test were performed. Three cubes (50 mm ×50 mm × 50 mm) for each mix were cast and tested in compression machine with 3,000 kN capacity under load control at a loading rate of 25 kN/min. Coupon specimens 300 mm × 75 mm × 12 mm were employed for bending test. All the specimens were cured in open air under humidity of 65% RH and temperature of 28°C conditions on average for 90 days.

3.3.2 Microstructural testing

(1) Wedge splitting test

Wedge splitting test (WST), originally introduced by Tschegg and Linsbauer in 1986 [19] and improved by Bruhwiler and Wittmann [20] is a suitable method for obtaining the fracture

energy and fracture toughness. In this research, WST method was used for the matrix toughness (same mix design as in Table 3 without the addition of fiber) based on the specimen size in [21] with its interpretation formulas as Eqns. (4)-(6) and the critical crack length procurement from cracking mouth opening displacement (CMOD) in [22] as Eqn. (3).

$$CMOD_c = \frac{P_c}{BE}\left[11.56\left(1-\frac{a_c}{D}\right)^{-2} - 9.397\right] \quad (3)$$

$$K_{ic} = (K_m) = \frac{P_c}{B\sqrt{D}}F(\propto) \quad (4)$$

$$F(\propto) = 29.6 \propto^{0.5} - 185.5 \propto^{1.5} + 665.7 \propto^{2.5} - 1017.0 \propto^{3.5} + 638.9 \propto^{4.5} \quad (5)$$

$$\alpha = \frac{a_c}{D} \quad (6)$$

where B is the thickness of the specimen, D is the depth of specimen, and a_c is the effective crack length. E is the elastic modulus of the matrix, P_c is the critical (peak) load, and $CMOD_c$ is the critical CMOD.

The loading device with specimen is displayed in Fig. 5. The loading machine used in the present study was INSTRON 5569 uniaxial testing system with the capacity of 50 kN. It was controlled by displacement with constant speed at 0.2 mm/min. The splitting force was applied onto the specimen through pulley wheels which requires being frictionless. A single central line support on the bottom of the specimen was selected to resist the vertical force component. CMOD was measured using special clip gauge with ±4 mm travel and fixed at the same height as the roller center.

Fig. 6 shows the geometry and size of the cube specimen. The initial notch that simulates the crack was made by inserting a steel plate of 1 mm thickness in the specimen during casting and taking out after one day curing. The notch depth was kept constant at 90 mm. Thereafter, all the specimens were cured in water for 90 days and dried in air one day before testing.

(2) Single fiber pullout test

Single fiber pullout tests were carried to study the influence of RCF content and particle size on fiber/matrix interface bond. The single fiber pullout test was conducted on an INSTRON 5569 uniaxial testing machine (UTM) at a speed of 0.06 mm/min. The whole setup was divided into four parts as can be seen from Fig. 7. From the bottom, an X-Y table with ±25 mm travel distance to two directions was fixed to the lower gripper of the UTM machine in order to ensure accurate fiber alignment. A 10 N load cell with 0.0001 N of accuracy was used to measure the pullout force. Samples were connected to the load cell through a T-shape sample holder with flat top surface to glue samples and a T bar to screw into the load cell. The embedded end of fiber should be avoided to glue to the sample holder since the pullout force would augment in that case. An aluminum plate, where the free end of the fiber was stuck, was clamped on the upper gripper. The free length of fiber was kept at 1 mm.

Fig. 8 shows the preparation of specimens for the single fiber pullout test. The embedment length was chosen to be around 1 mm to ensure full debonding and fiber pullout can occur. To obtain such small length, specimens were cut from thin mortar plates (20 mm × 50 mm × 5 mm) in which continuous fibers were embedded. The mortar matrix had the same mix design as in Table 3 without the addition of fibers.

Fiber/matrix interface bond can be determined from the single fiber pull-out curve. A variety of fiber pull-out models [23-25] are available to interpret the experimental data into interface bond properties. In the present research, bond properties of polyvinyl alcohol (PVA) fibers in a mortar matrix were investigated with a model described in [26], which can describe three

bond properties through the notions of the chemical bond G_d, the frictional bond τ_0 and slip hardening coefficient β.

4 Results and discussion

4.1 Compressive strength of RCF-ECC

The values of compressive strengths with varying RCF content and RCF size are showed in Table 4. Compared to the control group without RCF (RCF-0), ECC with fine RCF of 0~300 μm in Series 1 (RS-0.2-300) maintains the same level of compressive strength. This may be attributed to self-cementing properties of RCF which has been suggested in literatures [10, 27]. While the inclusion of fine RCF introduces more interface transition zones (ITZ), fine RCF may also possess higher content of unhydrated cement which improves the ITZ of the resulting RCF-ECC. Figure 9 shows the XRD results of RCFs with two particle sizes, i.e. < 300 μm and < 600 μm. As can be seen, more obvious peaks associated with compounds of CaO-SiO-AlO were detected in the finer RCF indicating more mortar existed in particles less than 300 μm. Furthermore, stronger C_2S peaks were also found in the finer particles, which suggest the presence of more unhydrated cement and potential stronger self-cementing of finer RCF particles.

When the maximum RCF size increases from 300 μm to 600 μm (RS-0.2-600), 20% compressive strength reduction is observed. Although the use of larger RCF reduces the amount of ITZ, self-cementing properties of larger RCF of 600 μm may decrease rapidly resulting in weaker ITZ and reduced compressive strength. With continuing increase of the RCF size, the compressive strength recovers to the level of above 50 MPa. This may be attributed to the greater reduction of the amount of weak ITZ and the influence of reduced self-cementing properties is not significant anymore. It should be noted that, in general, three

types of ITZ existed in concrete with recycled aggregates: the old ITZ between old mortar and natural aggregate; the new ITZ between old mortar and new cement paste; and the new ITZ between natural aggregate and the new cement paste. This is especially important for concrete with recycled coarse aggregates [28]. The recycled concrete fines; however, mainly consists of old mortar with very few natural aggregates [29, 30]. The major ITZ type in RCF-ECC of current study was believed to be the new ITZ between old mortar and new cement paste. In summary, self-cementing properties of RCF dominates the compressive strength of RCF-ECC when fine RCF is used while the amount of ITZ controls the compressive strength when larger size of RCF is used to produce RCF-ECC as shown in Fig. 10.

As for the impact of RCF content to compressive strength, the trend shows that the compressive strength reduces with increase of RCF content when RCF with maximum size of 600 μm is used. As discussed above, the contribution of RCF self-cementing diminishes rapidly with increasing RCF size and is not the dominated factor of RCF with maximum size of 600 μm. Therefore, the main cause of compressive strength reduction can be attributed to increased amount of ITZ with more RCF inclusion, which makes the composite less resistant to mechanical loads. Besides that, the porous adhered old mortar on the RCF surface can induce higher porosity, which also contributes to lower compressive strength of the composite.

4.2 Flexural behavior of RCF-ECC

Figs. 11 and 12 show the representative flexural stress versus deflection curves of Series 1 and Series 2 RCF-ECCs, respectively. As can be seen, all groups of specimens exhibit deflection-hardening with multiple cracking as shown in Fig. 13, which is the cracking state on the bottom surface of the specimen. Corresponding strain capacity of each group was

inversely calculated from the load-deflection curve according to Qian and Li [31] and was summarized in Table 4. Influence of RCF particle size on strain capacity of RCF-ECC is plotted in the same figure of compressive strength as Fig. 10. As can be seen, the effect of RCF particle size on strain capacity is the reverse of that on compressive strength. This suggests reduced matrix strength favors the formation of multiple cracking and enhances strain capacity of RCF-ECC. For series 2, both the flexural strength and strain capacity decrease with increasing RCF content. This is attributed to increased matrix toughness which is studied in detail in the following microstructural investigation.

As can be seen, inclusion of RCF may alter the performance of ECC. It is demonstrated, however, RCF-ECC can be designed to maintain their ductility provided the amount of RCF and particle size are properly controlled. To discover the underlying causes of performance difference, influence of RCF size and content on matrix and fiber/matrix interface was studied in the following section.

4.3 Influence of RCF on matrix toughness

Fig. 14 shows the typical failure mode of samples after the wedge splitting test, which breaks into two halves along the pre-notch. The test results of matrix toughness are summarized in Table 5. As can be seen, the addition of RCF both the size and the content show great influence on matrix toughness. Influence of RCF size on matrix toughness is similar to that on compressive strength, where it decreases first from 300 μm to 600 μm and increases afterwards. Based on crack trapping mechanism [32], matrix toughness increases with increased aggregate size because crack needs to make a longer detour to propagate through a larger aggregate and larger aggregate provides stronger mechanical anchoring to prevent

sliding of the fracture surfaces and to dissipate energy. The higher matrix toughness of RS-0.2-300 may be attributed to the self-cementing properties of fine RCF.

The matrix toughness of RCF-ECC increases with increased amount of RCF. Since the contribution of self-cementing is not the dominant factor for RCF with maximum size of 600 μm, increase of matrix toughness in this case is attributed to that fact that crack needs to propagate through more aggregates when more RCF is added to the matrix and therefore dissipating more energy. Similar phenomena on the influence of the inclusion of microsilica sand on matrix toughness was reported [17].

4.4 Influence of RCF on fiber/matrix interface

Table 6 summarized the fiber/matrix interface bonds obtained from the single fiber pullout test. As can be seen, chemical bond G_d decreases with increased particle size as shown in Fig. 15(a). Chemical bond describes adhesion between fiber and matrix. Higher G_d suggests stronger chemical structure between the fiber surface and the mortar matrix when smaller RCF particles are used, perhaps due to the self-cementing property of fine RCF which enhances the interface chemical adhesion. Reduced G_d generally increases the complimentary energy J_b' of fiber bridging which favors multiple cracking of ECC.

Frictional bond τ_0 first decreases with increased particle size followed by a reverse trend when large RCF is used as shown in Fig. 15(b). Frictional bond represents mechanical friction between fiber and matrix. As discussed above, the use of fine RCF (RS-0.2-300) results in higher matrix toughness due to self-cementing of fine RCF. The inclusion of coarse RCF (RS-0.2-2360) on the other can also improve toughness of the surrounding matrix as shown in Table 5 and reproduced in Fig. 15(b). Both can lead to higher mechanical friction

between fiber and matrix. The moderate frictional bond within 1~2MPa is anticipated to achieve better strain-hardening behavior due to a balanced fiber pullout and rupture behavior which maximized the complimentary energy J_b' and strength σ_B of fiber bridging [33].

Slip hardening coefficient β also decreases with increased particle size first followed by a reverse trend when large RCF is used as shown in Fig. 15(c). Slip hardening captures the phenomenon of soft polymer fiber scrapped by the surrounding hard matrix during sliding. Higher β shows that fibers are damaged more due to tougher matrix and higher interfacial friction. As mentioned, both the use of fine RCF (RS-0.2-300) or coarse RCF (RS-0.2-2360) can lead to harder matrix resulting in higher β.

With regard to the influence of RCF content as Fig.16, the general trend shows that G_d and β decrease while τ_0 slightly increases with increased RCF content. The inclusion of higher content of RCF reduces the over binder content and therefore chemical adhesion between fiber and matrix reduces as well. Higher RCF content enhances matrix toughness which can lead to higher mechanical friction.

4.5 Influence of RCF on ECC tensile strain-hardening behavior

Based on the measured interface properties in the section 4.4, influence of RCF size or content on fiber bridging σ(δ) curve and J_b' can be calculated through the numerical process proposed by Yang et al. [16]. Effects of RCF size on fiber bridging and pseudo strain-hardening (PSH) indices (J_b'/J_{tip}) are shown in Fig. 17. As can be seen, both the stiffness and the peak strength of the fiber bridging first decreases with the increase of RCF size followed by a reverse trend when large RCF is used similar to the friction bond τ_0. The complementary energy J_b', also shows a similar trend by taking into account all component properties into the

model as shown in Fig. 17(b). PSH indices were calculated based on the information obtained from Fig. 17(a) and Table 5. A PSH index beyond 1.0 indicates potential strain-hardening performance and a larger PSH index gives higher chance for saturated multiple cracking and higher strain capacity. As can be seen in Fig. 17(b), all RCF-ECCs have PSH indices larger than one and RCF-0.2-600 has the highest PSH index. This conclusion corresponds well with the measured composite performance as most of the RCF-ECCs have strain capacity above 1% (Table 4). Thereof, RS-0.2-600 exhibits the highest strain capacity of 2.03% with the formation of saturated multiple cracks.

Influence of RCF content on fiber bridging and PSH indices are shown in Fig. 18. As can be seen, the stiffness of bridging curve and peak bridging strength increase while the complementary energy J_b' decreases with the increase of RCF content due to increase of friction bond and decrease of chemical bond as shown in Fig. 16. While the PSH reduces with the increase of RCF content, all RCF-ECCs still have PSH indices larger than one. This again corresponds well with the composite performance where the strain capacity reduces with the increase of RCF content and all three RCF-ECCs have strain capacity above 1.5%. The addition of excessive RCF can lead to reduced tensile ductility with less saturated multiple cracking as shown in Table 4.

5. Conclusions

This study investigated potential use of recycled concrete fines (RCF) as microsilica sand substitute in the production of ECC. Experiments were carried out in the composite level and in the component level to reveal the influence of RCF size or content on the mechanical properties as well as matrix and fiber/matrix interface properties of the resulting RCF-ECCs.

Micromechanical model was engaged to calculate the resulting fiber bridging $\sigma(\delta)$ curves and the influence of RCF size and content on tensile strain-hardening of RCF-ECC was revealed. Inclusion of RCF may alter the performance of ECC. All RCF-ECCs produced in this study; however, still possessed decent compressive strength above 40 MPa with strain capacity more than 0.8%. It is therefore viable to use recycled concrete fines (RCF) as microsilica sand substitute in the production of ECC. Microstructure investigation on the component level revealed that RCF size and content modify matrix toughness and fiber/matrix interface properties due to various mechanisms including self-cementing of fine RCF. The fiber bridging $\sigma(\delta)$ curves as well as PSH indices can then be determined by the micromechanical model. The results clearly explained the influence of RCF size and content on ECC properties. Micromechanics-based design principle can be used for ingredients selection and component tailoring of RCF-ECCs.

Acknowledgement

This research grant is supported by the Singapore National Research Foundation under its Environmental & Water Technologies Strategic Research Programme and administered by the Environment & Water Industry Programme Office (EWI) of the PUB.

References

1. Sagoe-Crentsil KK, Brown T, and Taylor AH. Performance of concrete made with commercially produced coarse recycled concrete aggregate. Cem Concr Res 2001; 31: 707-712.

2. Katz A. Treatments for the improvement of recycled aggregate. J Mater Civ Eng, ASCE 2004; 16(6): 597-603.

3. Kou S-c, Poon C-s, and Agrela F. Comparisons of natural and recycled aggregate concretes prepared with the addition of different mineral admixtures. Cem Concr Compos 2011; 33(8): 788-795.

4. Tam VWY, Gao XF, and Tam CM. Microstructural analysis of recycled aggregate concrete produced from two-stage mixing approach. Cem Concr Res 2005; 35(6): 1195-1203.

5. Katz A and Baum H. Effect of high levels of fines content on concrete properties. ACI Mater J 2006; 103(6): 474-482.

6. Meyer C. The greening of the concrete industry. Cem Concr Compos 2009; 31(8): 601-605.

7. Ravindrarajah RS and Tam CT. Recycling concrete as fine aggregate in concrete. Int J Cem Compos Lightweight Concr 1987; 9(4): 235-241.

8. Khatib JM. Properties of concrete incorporating fine recycled aggregate. Cem Concr Res 2005; 35(4): 763-769.

9. Evangelista L and de Brito J. Mechanical behaviour of concrete made with fine recycled concrete aggregates. Cem Concr Compos 2007; 29(5): 397-401.

10. Kou SC and Poon CS. Properties of self-compacting concrete prepared with coarse and fine recycled concrete aggregates. Cem Concr Compos 2009; 31(9): 622-627.

11. Yaprak H, et al. Effects of the fine recycled concrete aggregates on the concrete properties. Int. J. Phys. Sci 2011; 6(10): 2455-2461.

12. Li VC. On Engineered Cementitious Composites (ECC)-A review of the material and its applications. J Adv Concr Technol 2003; 1(3): 215-230.

13. Yang EH and Li VC. Strain-hardening fiber cement optimization and component tailoring by means of a micromechanical model. Constr Build Mater 2010; 24(2): 130-139.

14. Lepech MD, et al. Design of green Engineered Cementitious Composites for improved sustainability. ACI Mater J 2008; 105(6): 567-575.

15. Marshall D and Cox BN. A J-integral method for calculating steady-state matrix cracking stresses in composites. Mech Mater 1988; 7: 127-133.

16. Yang EH, et al. Fiber-bridging constitutive law of Engineered Cementitious Composites. J Adv Concr Technol February 2008; 6(1): 181-193.

17. Li VC, Mishra DK, and Wu H-C. Matrix design for pseudo-strain-hardening fibre reinforced cementitious composites. Mater Struct 1995; 28: 586-595.

18. Neville AM, Properties of concrete, 4th ed. London: Addison Wesley Longman Limited, 1995

19. Linsbauer HN and Tschegg EK. Fracture energy determination of concrete with cube shaped specimens. Zement und Beton 1986; 31: 38-40.

20. Brohwiler E and Wittmann FH. The wedge spliting test, a new method of performing stable fracture mechanics tests. Eng Fract Mech 1990; 35(1/2/3): 117-125.

21. Zhao GF, Jiao H, and Xu SL. Behavior with wedge splitting test method. In: van Mier JGM, et al.,editor. Fracture process in Concrete, Rock and Ceramics. London: E & FN Spon, 1991. p. 789-798.

22. Kim YY, et al. ECC produced with granulated blast furnace slag. Available from: http://citeseerx.ist.psu.edu/viewdoc/download?doi=10.1.1.146.5213&rep=rep1&type=pdf.

23. Gao YC. Debonding along the interface of composites. Mech Res Commun 1987; 14(2): 67-72.

24. Stang H, Li Z, and Shah SP. Pullout problem stress versus fracture mechanical approach. J Eng Mech, ASCE 1990; 116(10): 2136-2150.

25. Hsueh C-H. Evaluation of interfacial shear strength, residual clamping stress and coefficient of friction for fiber-reinforced ceramic composites. Acta metall mater 1990; 38(3): 403-409.

26. Redon C, et al. Measuring and modifying interface properties of PVA fibers in ECC matrix. J Mater Civ Eng, ASCE November/December 2001: 399-406.

27. Poon CS, Qiao XC, and Chan D. The cause and influence of self-cementing properties of fine recycled concrete aggregates on the properties of unbound sub-base. Waste Manage 2006; 26: 1166-1172.

28. Li WG, Xiao JZ, Sun ZH, Kawashimab S, Shah SP. Interfacial transition zones in recycled aggregate concrete with different mixing approaches. Constr Build Mater 2012; 35: 1045-1055.

29. Poon CS, Shui ZH, and Lam L. Effect of microstructure of ITZ on compressive strength of concrete prepared with recycled aggregates. Constr Build Mater 2004; 18(6): 461-468.

30. Florea MVA and Brouwers HJH. Properties of various size fractions of crushed concrete related to process conditions and re-use. Cem Concr Res 2013; 52: 11-21.

31. Qian S and Li VC. Simplified inverse method for determining the tensile strain capacity of strain hardening cementitious composites. J Adv Concr Technol 2007; 5(2): 235-246.

32. Li VC. Crack trapping and bridging as toughening mechnisms in high strength concrete. International Conference on micromechanics of Failure of Quasi-brittle Materials. 1990. p. 579-588.

33. Li VC, et al. Interface tailoring for Strain-Hardening Polyvinyl Alcohol-Engineered Cementitious Composite(PVA-ECC). ACI Mater J 2002; 99(5): 463-472.

Table 1 Properties of PVA fiber

Table 2 Physical properties of RCF

Table 3 Mix proportions of RCF-ECCs

Table 4 Mechanical Properties of RCF-ECCs

Table 5 Influence of RCF size and content on matrix toughness

Table 6 Influence of RCF size and content on interface properties

Table 1 Properties of PVA fiber

Diameter d_f (mm)	Tensile strength σ_t (MPa)	Elongation ε_f (%)	Young's modulus E_f (GPa)
0.044	1640	5.3	41.1

Table 2 Physical properties of RCF

Particle size (μm)	Density (g/cm^3)	Water absorption (%)	Fineness modulus	Average particle size (μm)
0~300	2.07	12.5	1.58	154
0~600	2.01	11.6	2.12	285
0~1180	1.94	10.0	2.51	542
0~2360	1.90	8.4	2.78	1074

Table 3 Mix proportions of RCF-ECCs (kg/m^3)

	Mix	Cement	Slag	Water	RCF	Fiber	SP	RCF size (μm)
Series 1	RS-0.2-300	286	1143	358	286	26	11	0~300
	RS-0.2-600	285	1138	356	285	26	11	0~600
	RS-0.2-1180	283	1132	354	283	26	11	0~1180
	RS-0.2-2360	282	1129	353	282	26	11	0~2360
Series 2	RS-0	333	1330	416	0	26	5	0~600
	RS-0.2-600	285	1138	356	285	26	11	0~600
	RS-0.5-600	234	936	292	585	26	14	0~600

1. B (binder) = Cement + Slag.

Table 4 Mechanical Properties of RCF-ECCs

	Mix	Compressive strength (MPa)	Flexural strength (MPa)	Strain capacity* (%)
Series 1	RS-0.2-300	52.96±3.39	6.30±1.17	1.64±0.63
	RS-0.2-600	42.44±3.13	6.90±1.57	2.03±0.25
	RS-0.2-1180	50.08±4.16	6.14±0.90	1.27±0.13
	RS-0.2-2360	50.53±4.04	4.90±0.83	0.88±0.10
Series 2	RS-0	52.45±3.59	6.12±0.50	2.30±0.11
	RS-0.2-600	42.44±3.31	6.90±1.57	2.03±0.25
	RS-0.5-600	40.49±5.24	6.18±0.92	1.60±0.42

*inversely calculated from the load-deflection curve [28]

Table 5 Influence of RCF size and content on matrix toughness

	Mix	P_c (N)	*CMOD* (m)	K_m (MPa•m$^{1/2}$)	J_{tip} (J/m^2)
Series 1	RS-0.2-300	1198	0.0550	0.54±0.03	14.60±1.84
	RS-0.2-600	1050	0.0491	0.48±0.02	11.52±1.02
	RS-0.2-1180	1312	0.0511	0.53±0.03	13.93±1.47
	RS-0.2-2360	1820	0.0541	0.61±0.03	18.31±1.96
Series 2	RS-0	878	0.0456	0.43±0.03	9.27±1.38
	RS-0.2-600	1050	0.0491	0.48±0.02	11.52±1.02
	RS-0.5-600	1594	0.0480	0.54±0.01	14.33±0.40

Table 6 Influence of RCF size and content on interface properties

	Mix	G_d (J/m^2)	τ_0 (MPa)	β	J_b' (J/m^2)
Series 1	RS-0.2-300	1.51±1.30	2.01±1.21	0.37±0.08	22.20
	RS-0.2-600	0.72±0.29	1.82±0.72	0.24±0.06	24.82
	RS-0.2-1180	0.39±0.29	1.94±0.06	0.25±0.10	25.84
	RS-0.2-2360	0.19±0.20	2.38±0.65	0.28±0.07	24.71
Series 2	RS-0	0.90±0.68	1.60±1.02	0.40±0.26	27.91
	RS-0.2-600	0.72±0.29	1.82±0.72	0.24±0.06	24.82
	RS-0.5-600	0.59±0.64	2.02±0.77	0.22±0.02	24.50

Figure 1 Grading curves of RCF

Figure 2 SEM images of RCF particles and micro-silica sand

Figure 3 SEM images of crushed aggregate particle

Figure 4 SEM images of hydrated cement product

Figure 5 Test setup of the wedge splitting test

Figure 6 Specimens for the wedge splitting test

Figure 7 Test setup of the single fiber pullout test

Figure 8 Specimens for the single fiber pullout test

Figure 9 X-ray diffraction patterns of RCF with particle size below 300 μm and 600 μm

Figure 10 Compressive strength & strain capacity vs. RCF size

Figure 11 Influence of RCF size on flexural behaviors of RCF-ECCs

Figure 12 Influence of RCF content on flexural behaviors of RCF-ECCs

Figure 13 Crack patterns of specimens

Figure 14 The failure mode of wedge splitting specimens

Figure 15 Influence of RCF size on fiber/matrix interface

Figure 16 Influence of RCF content on fiber/matrix interface

Figure 17 Effect of RCF size on (a) fiber bridging and (b) PSH indices

Figure 18 Effect of RCF content on (a) fiber bridging and (b) PSH indices

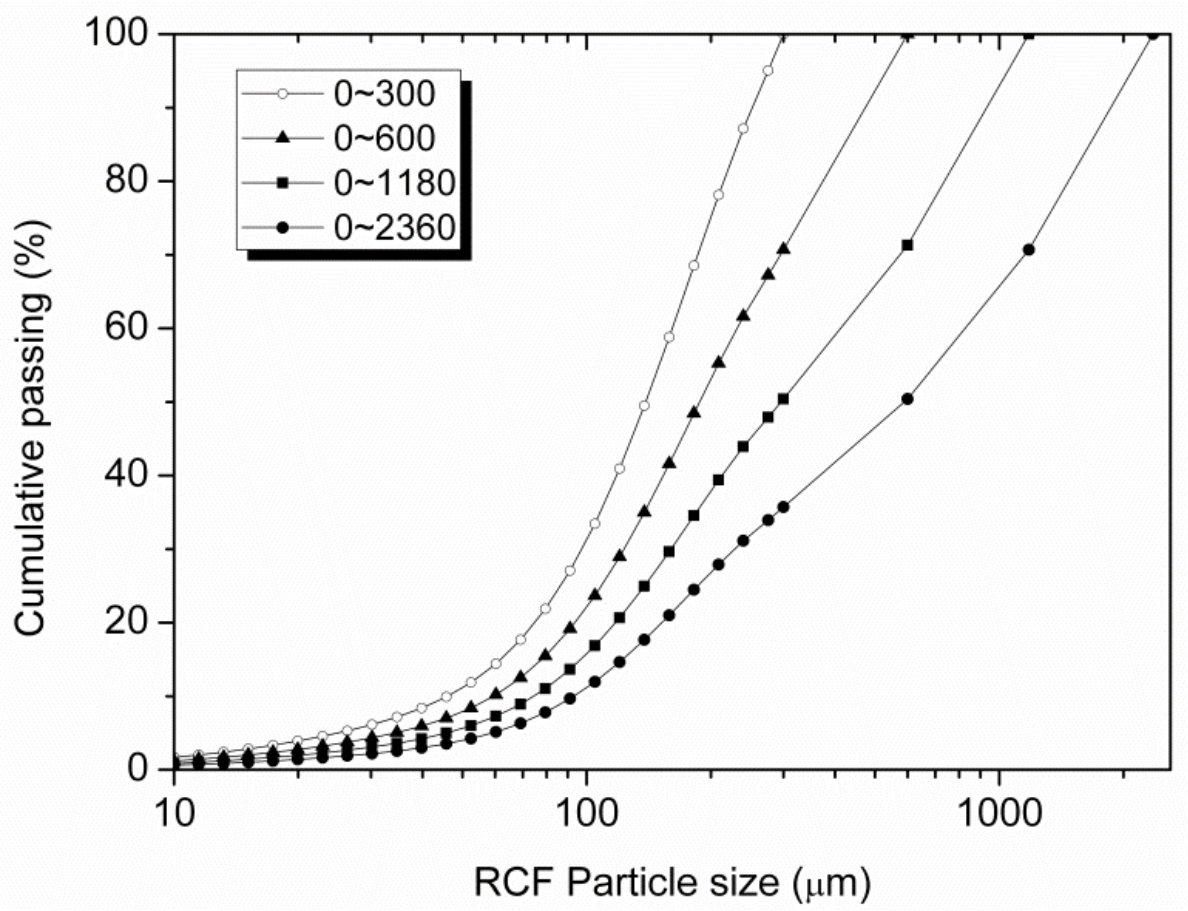

Figure 1 Grading curves of RCF

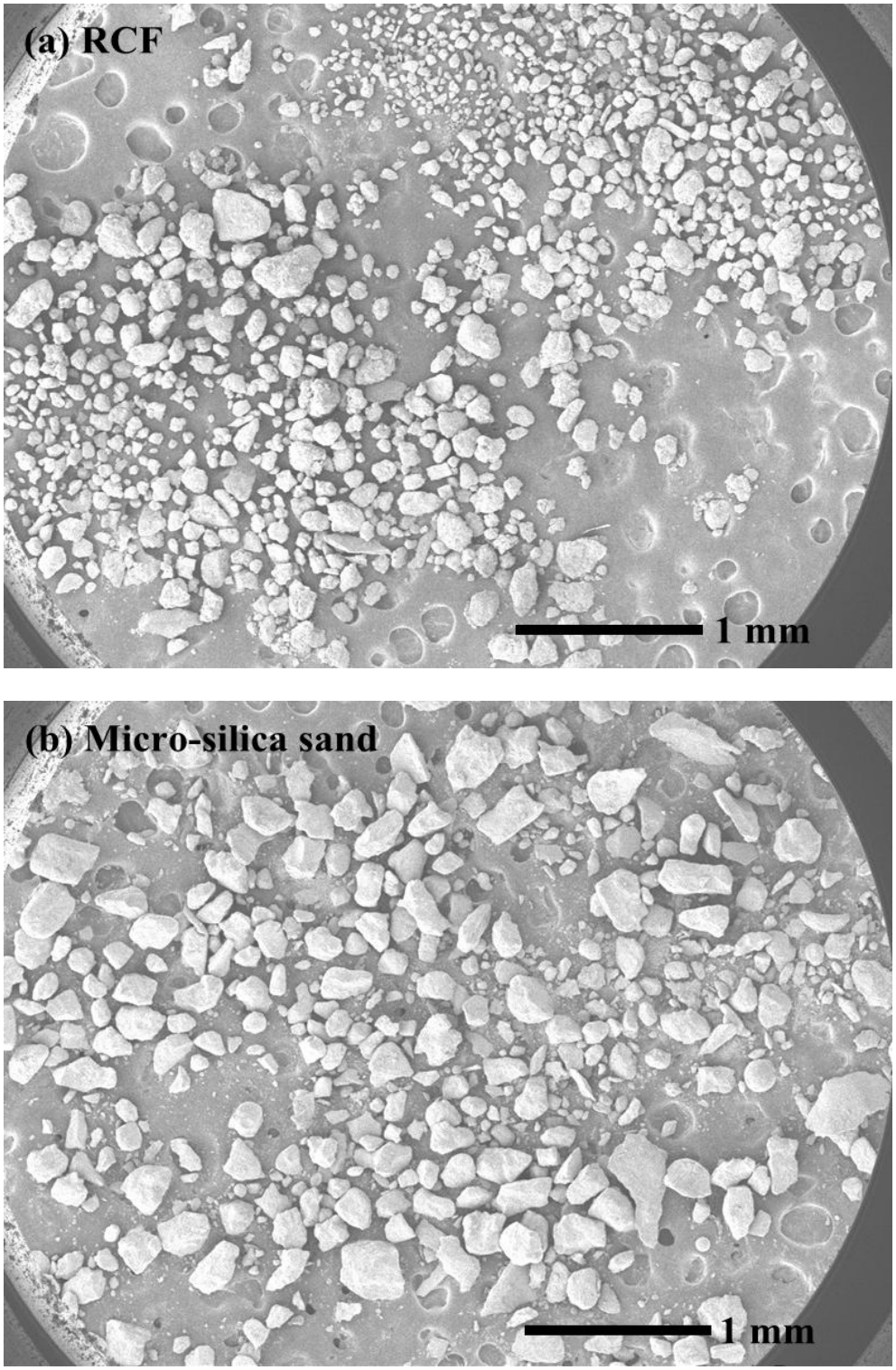

Figure 2 SEM images of (a) RCF particles, and (b) micro-silica sand

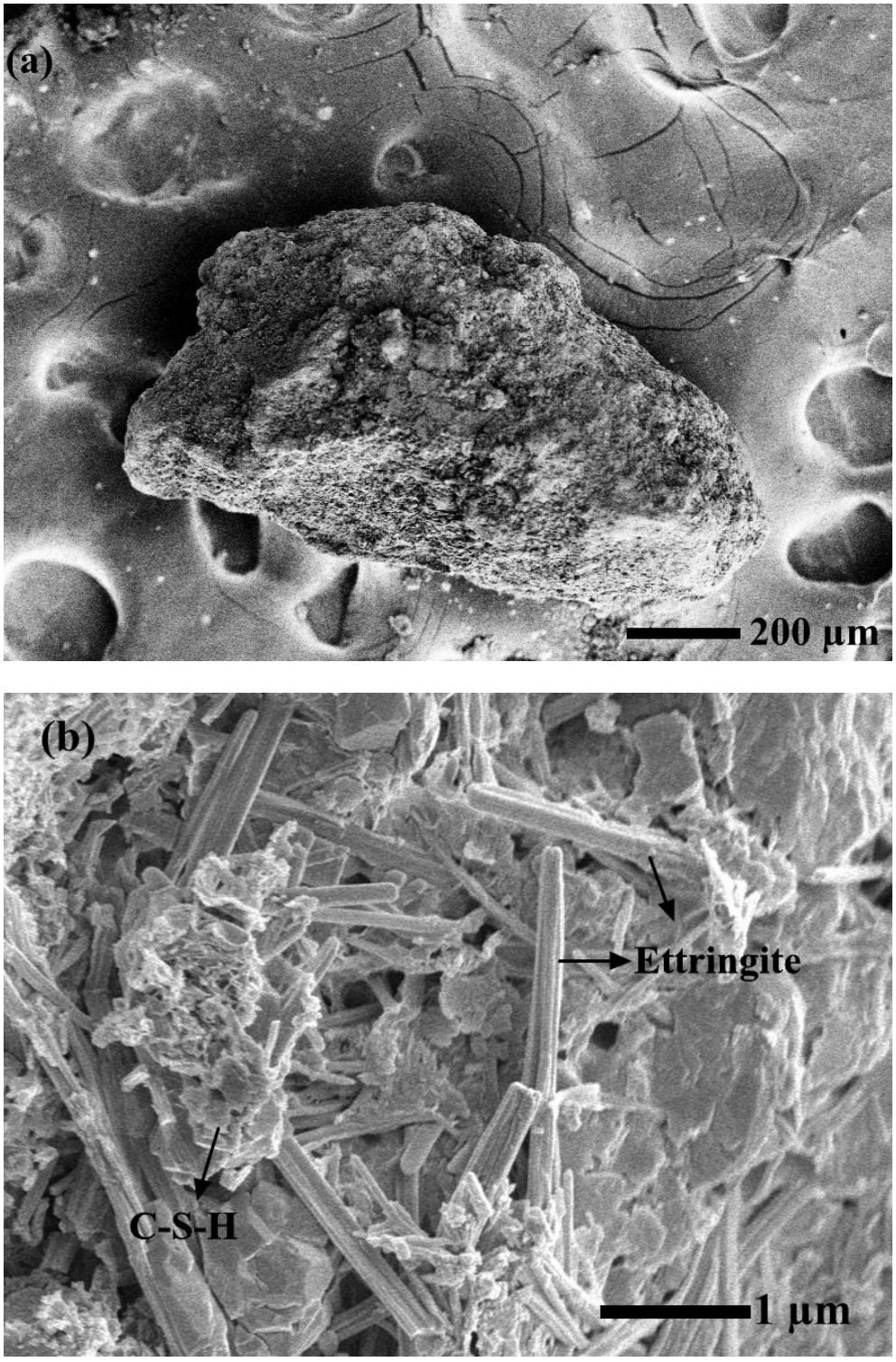

Figure 3 SEM images of (a) the crushed aggregate particle, and (b) the surface of the particle

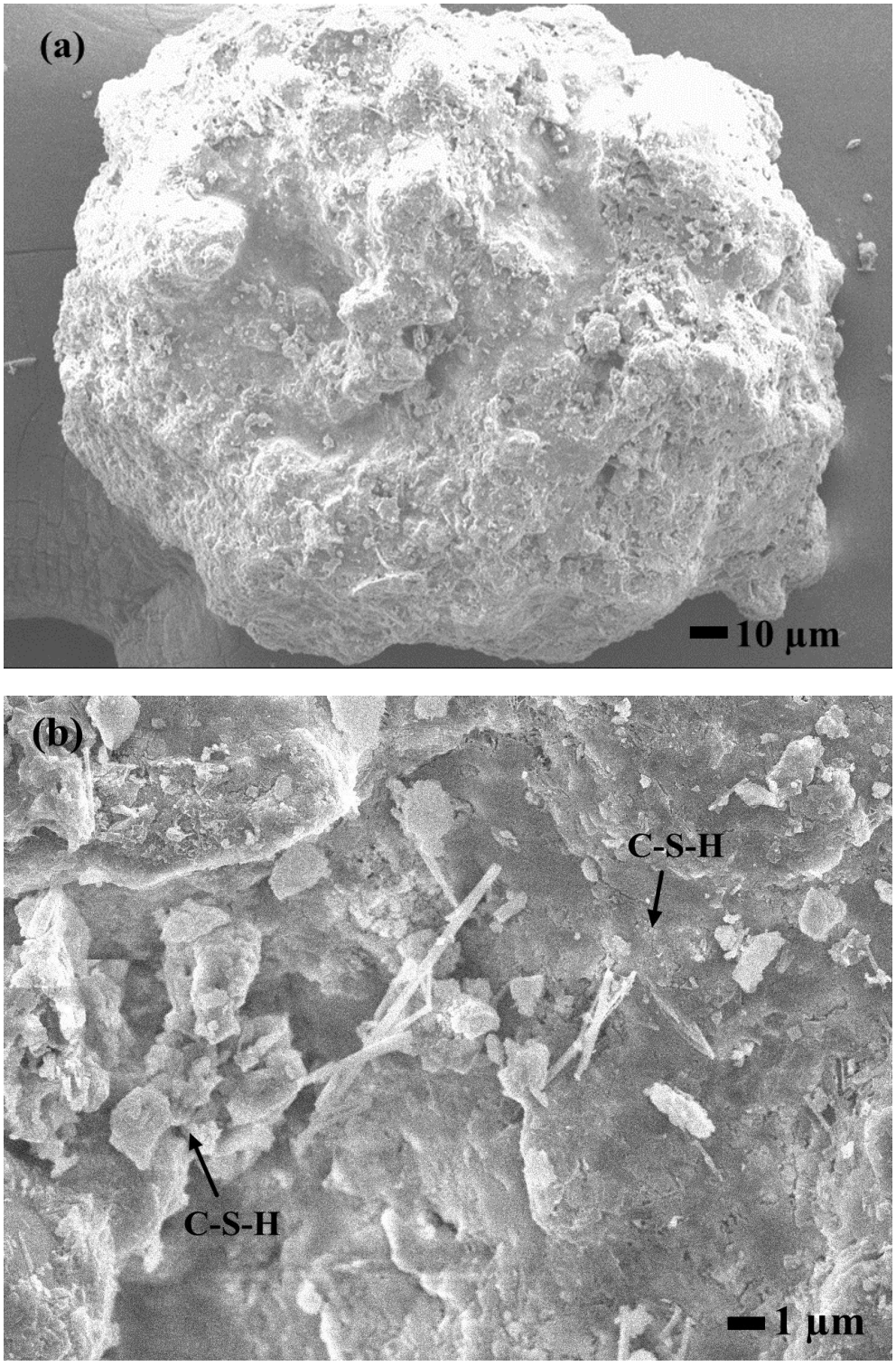

Figure 4 SEM images of (a) C-S-H particle, and (b) the surface of the particle

Figure 5 Test setup of the wedge splitting test

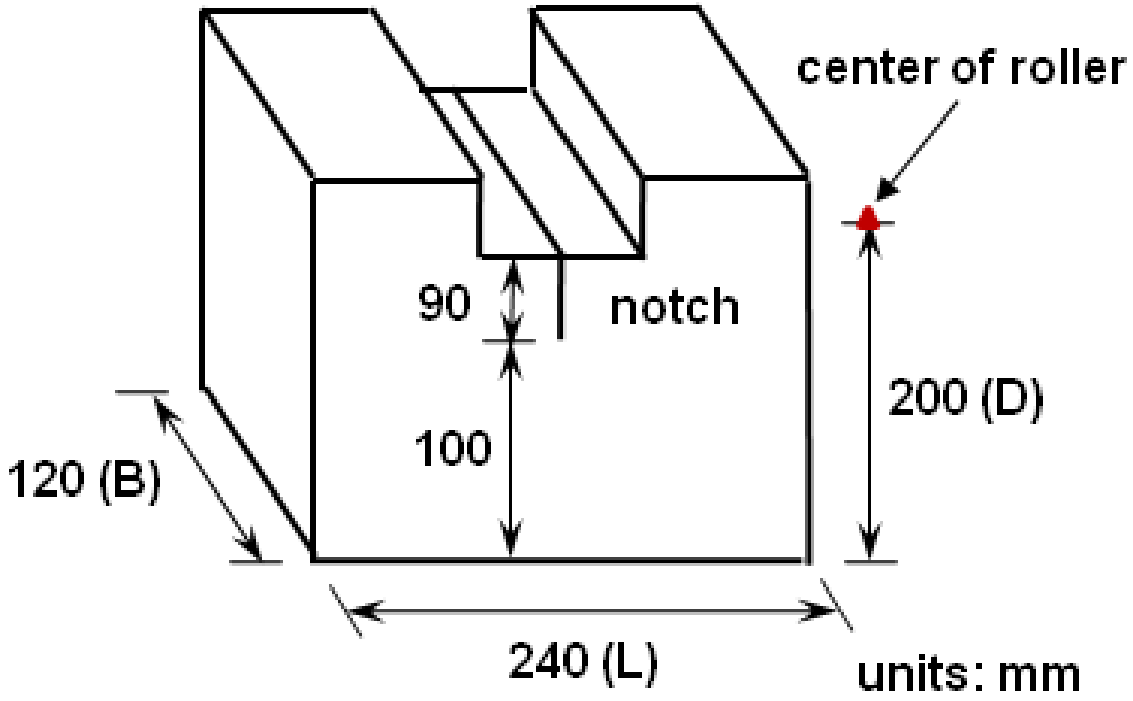

Figure 6 Specimens for the wedge splitting test

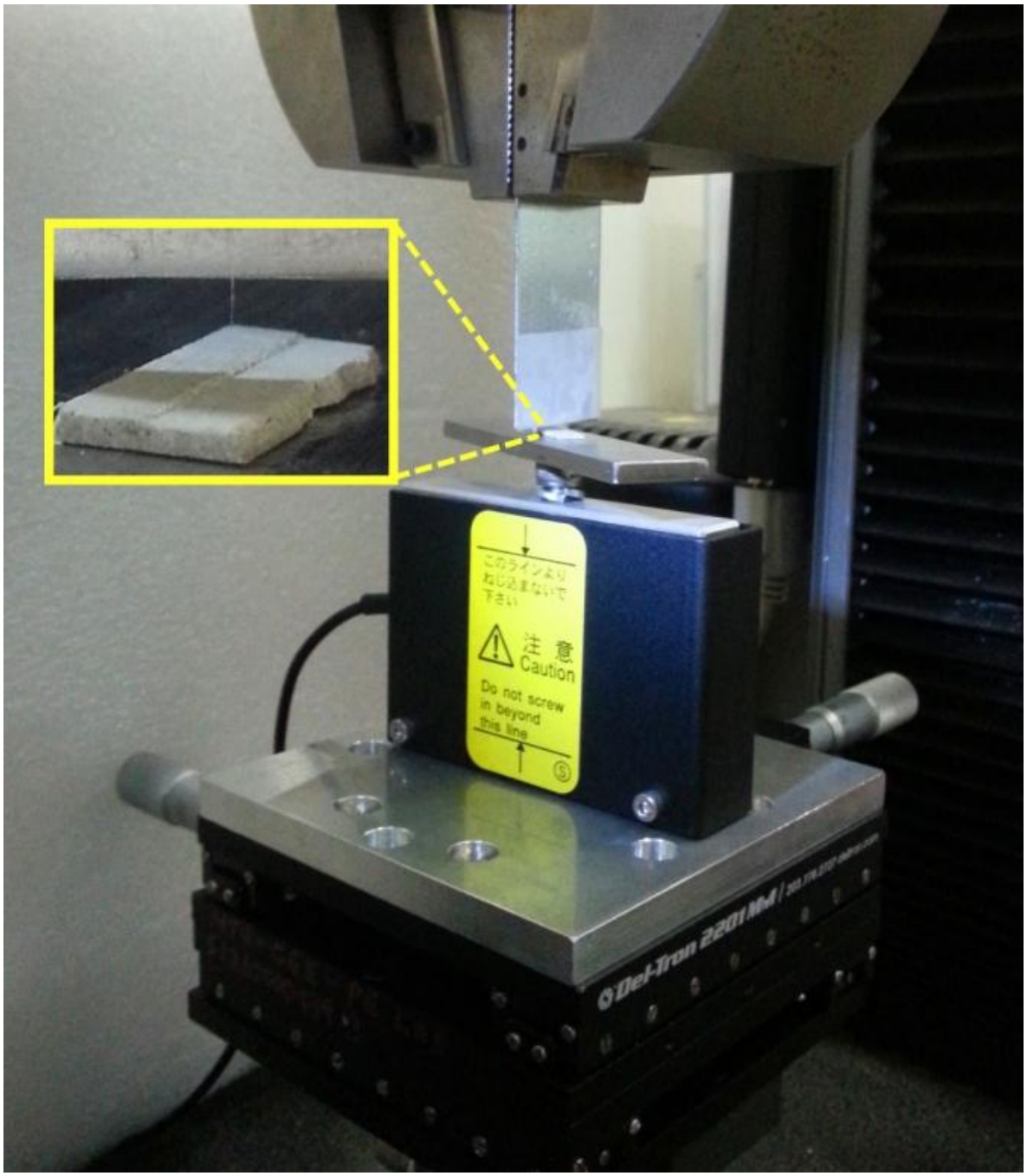

Figure 7 Test setup of the single fiber pullout test

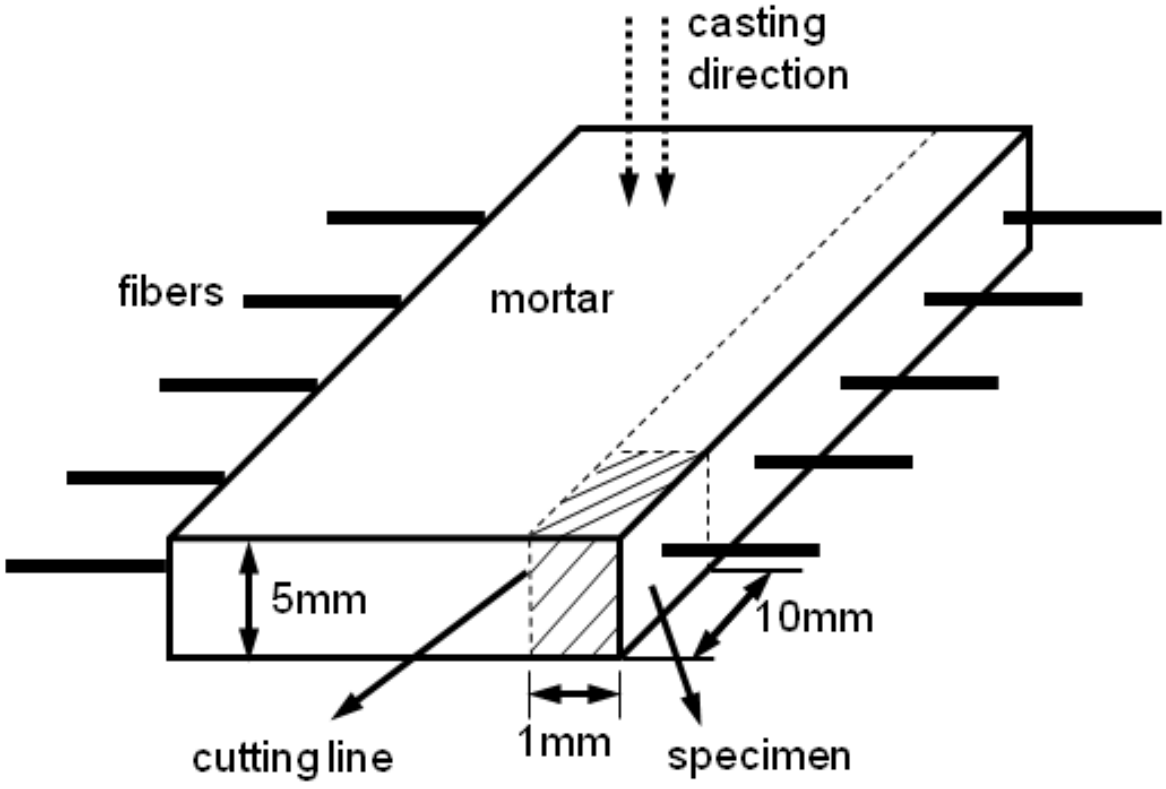

Figure 8 Specimens for the single fiber pullout test

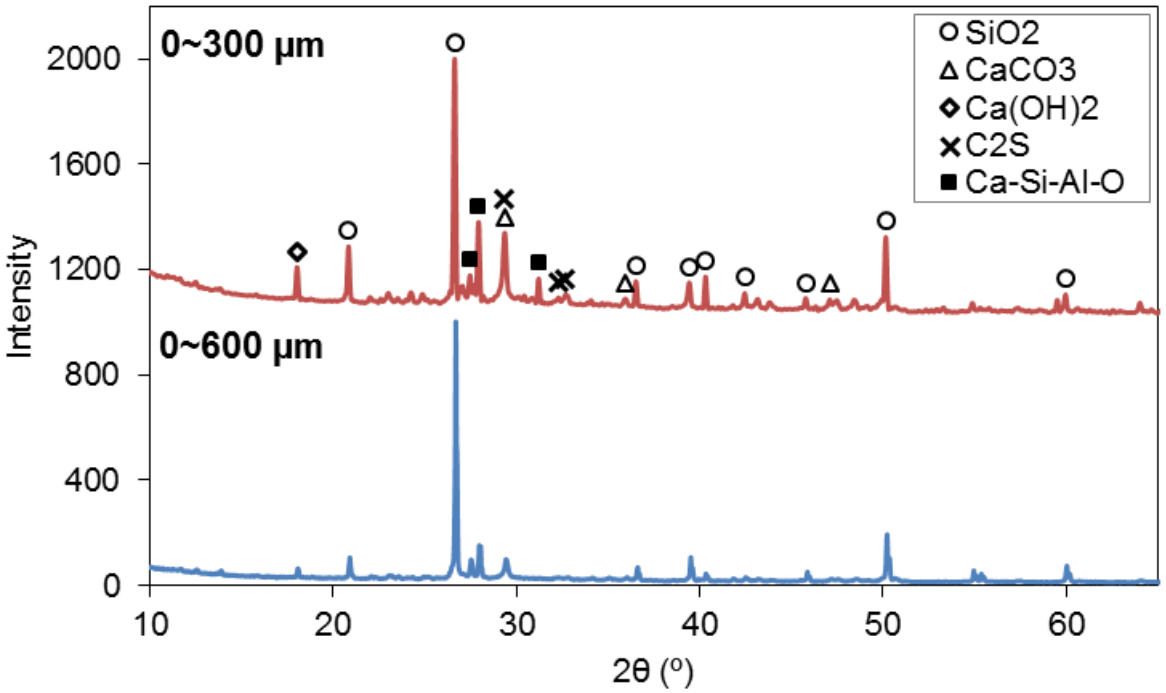

Figure 9 X-ray diffraction patterns of RCF with particle size below 300 μm and 600 μm

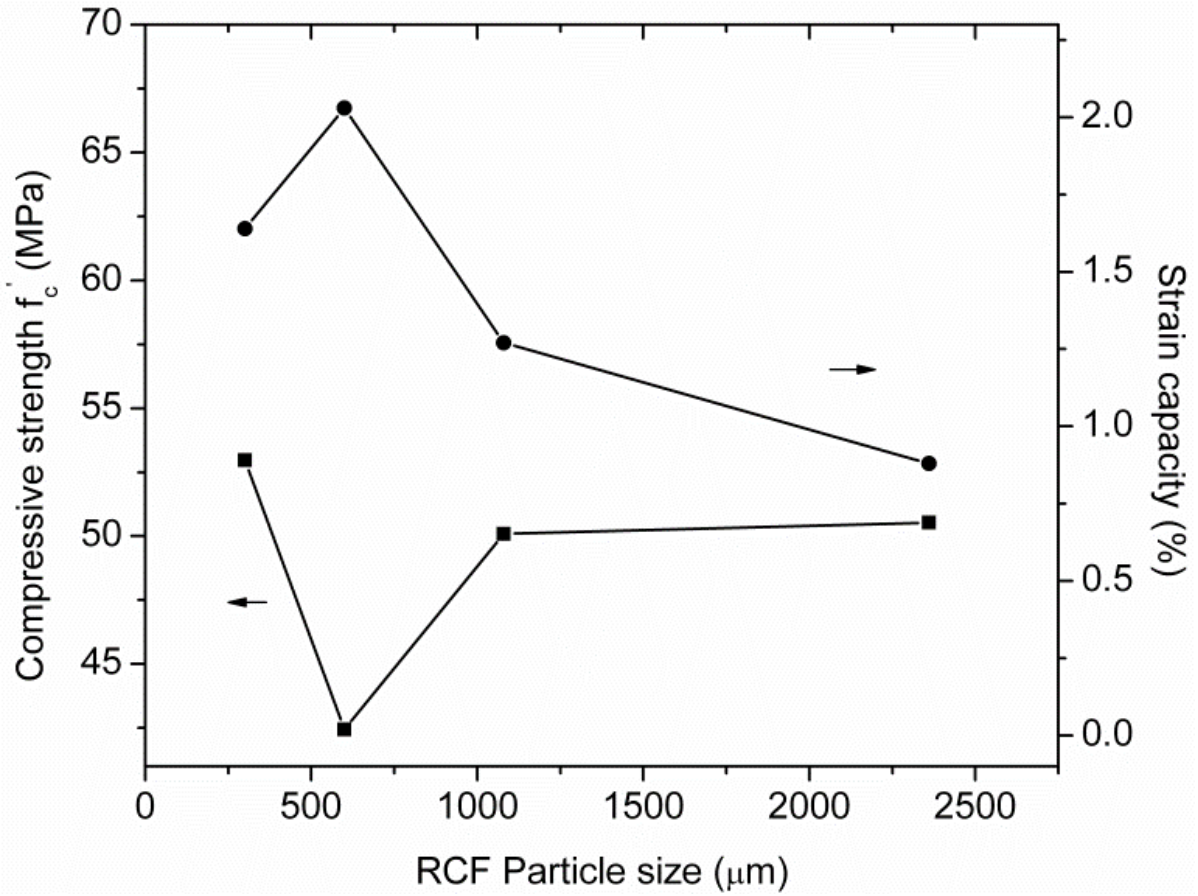

Figure 10 Compressive strength & strain capacity vs. RCF size

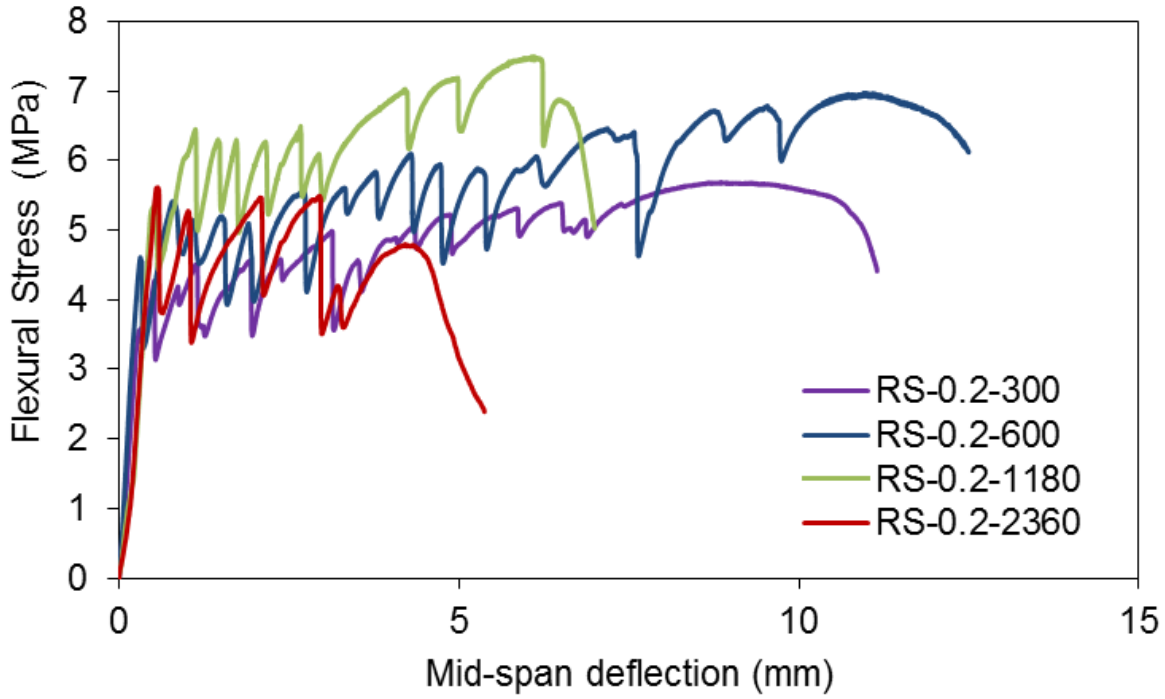

Figure 11 Influence of RCF size on flexural behaviors of RCF-ECCs

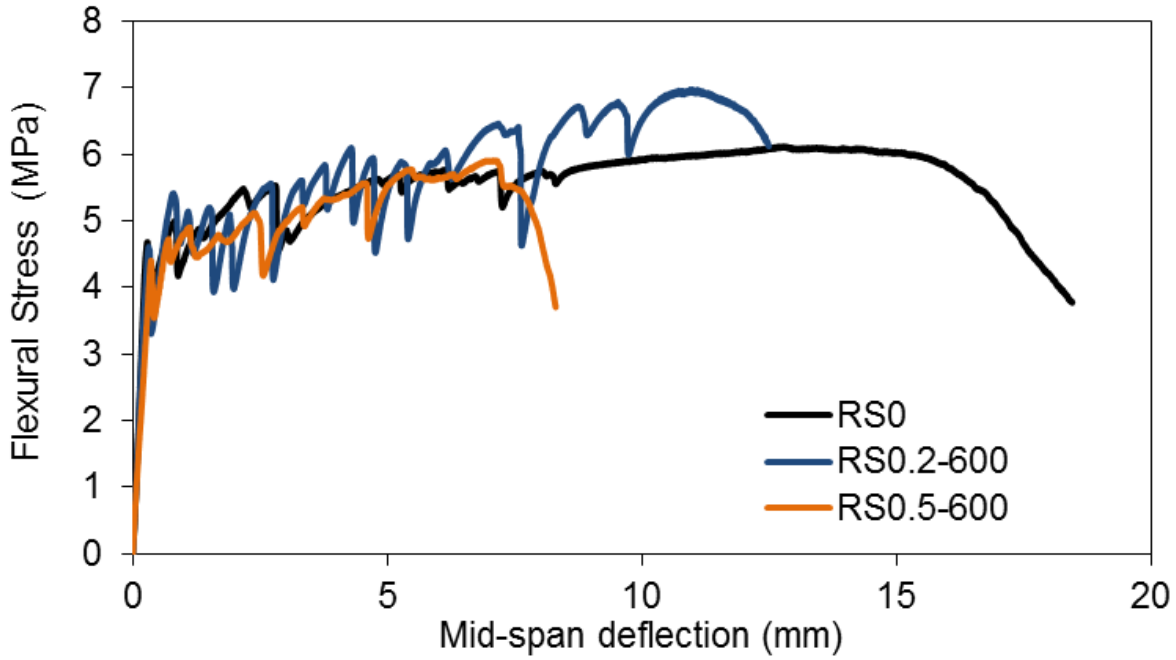

Figure 12 Influence of RCF content on flexural behaviors of RCF-ECCs

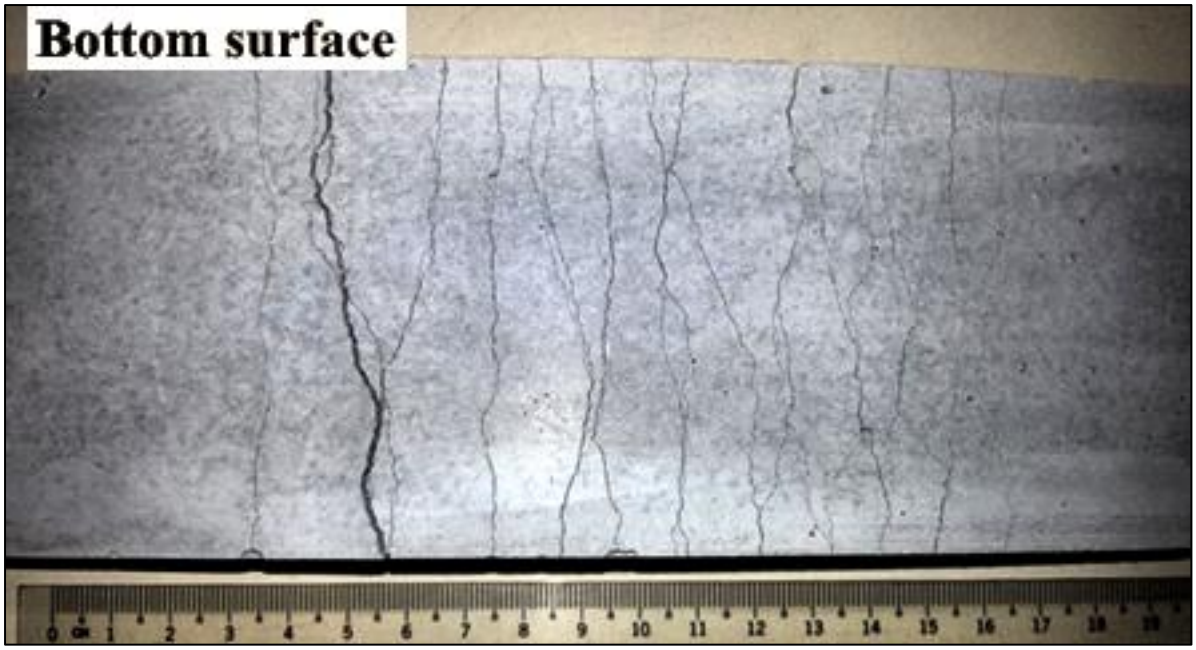

Figure 13 Crack patterns of specimens

Figure 14 The failure mode of wedge splitting specimens

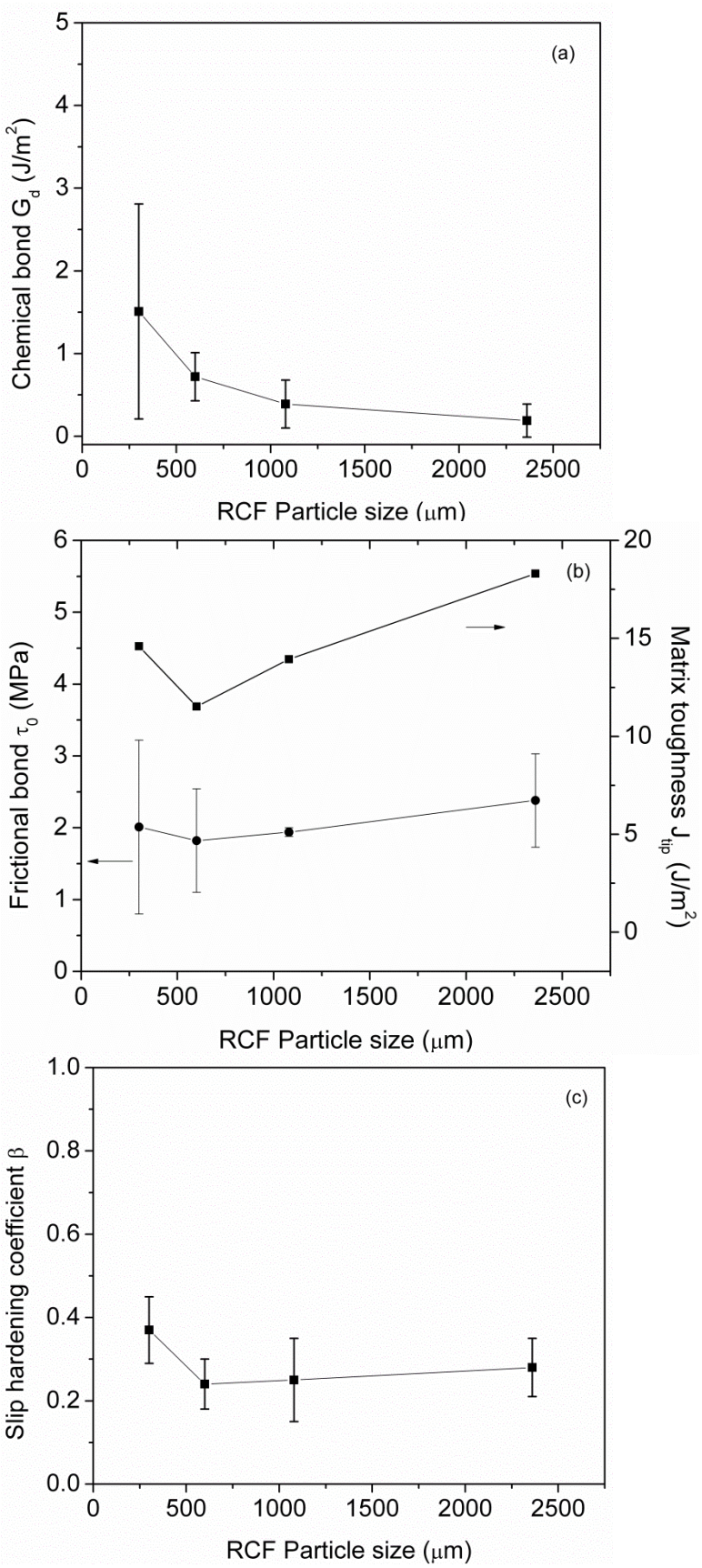

Figure 15 Influence of RCF size on fiber/matrix interface

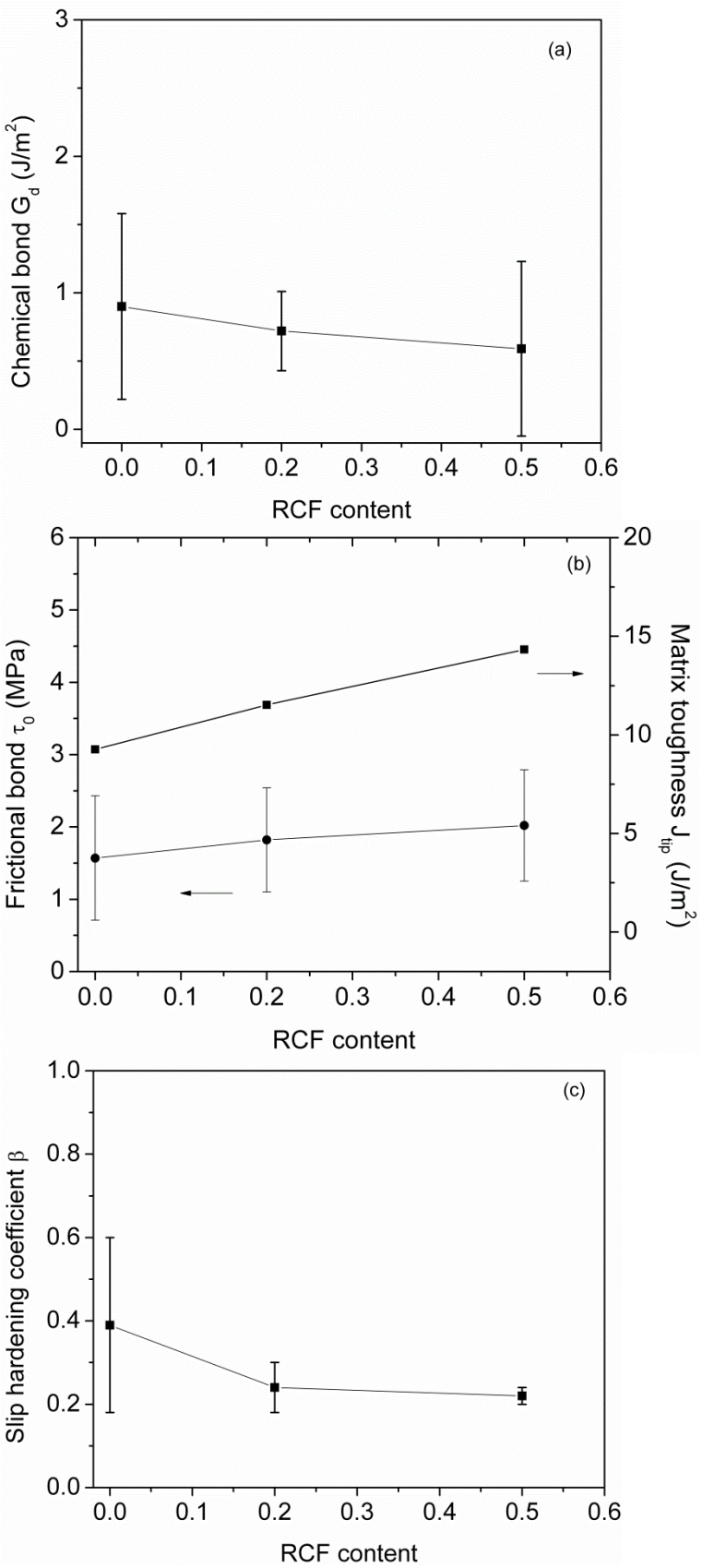

Figure 16 Influence of RCF content on fiber/matrix interface

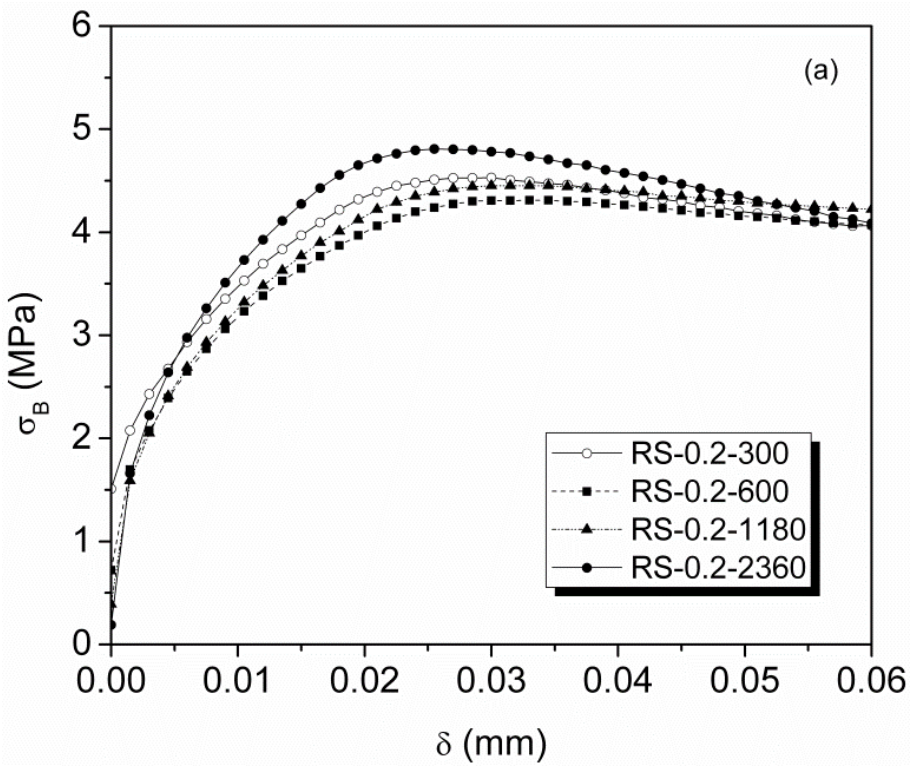

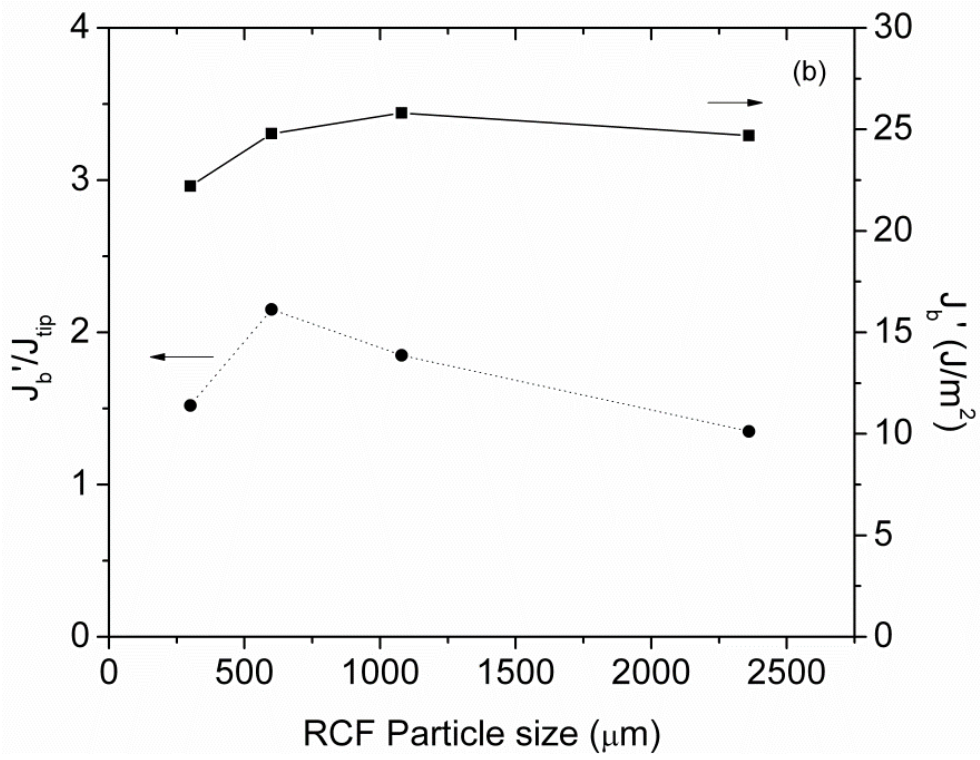

Figure 17 Effect of RCF size on (a) fiber bridging and (b) PSH indices

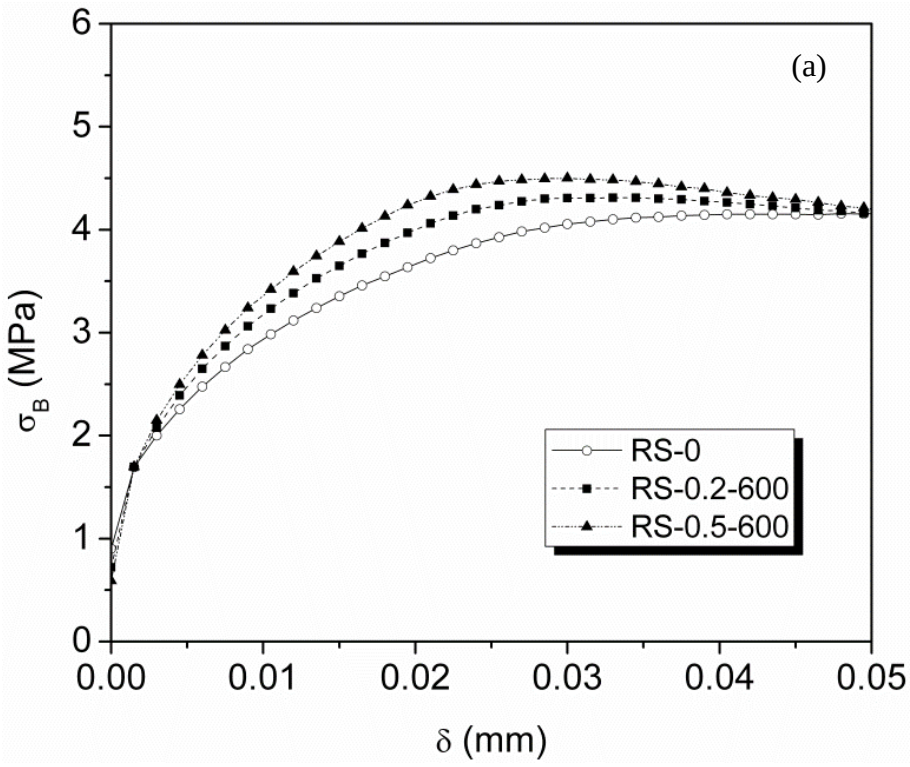

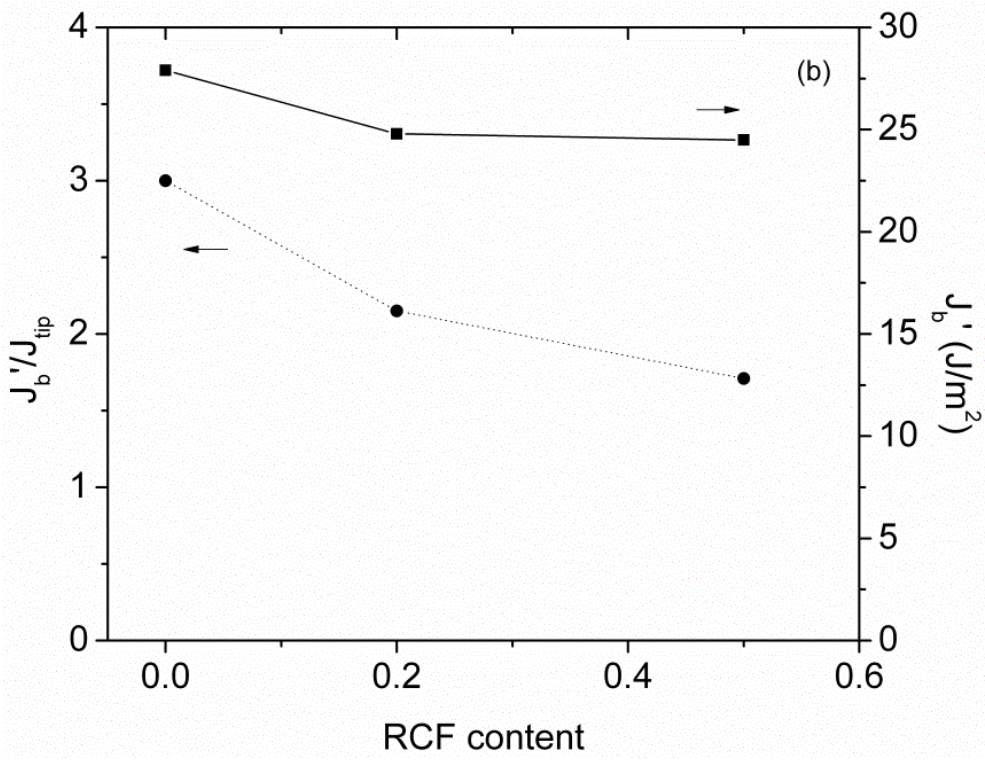

Figure 18 Effect of RCF content on (a) fiber bridging and (b) PSH indices

Macroscopic and Microstructural Properties of Engineered Cementitious Composites Incorporating Recycled Concrete Fines

Junxia Li[a,b], En-Hua Yang[c,1]

[a]Interdisciplinary Graduate School, Nanyang Technological University, 50 Nanyang Avenue, Singapore 639798

[b]Residues & Resource Reclamation Centre, Nanyang Environment and Water Research Institute, Nanyang Technological University, 1 Cleantech Loop, Singapore 637141

[c]School of Civil and Environmental Engineering, Nanyang Technological University, 50 Nanyang Avenue, Singapore 639798

ABSTRACT

Recycled concrete fines (RCF) are fine aggregates and particles from the demolition waste of old concrete. Unlike recycled coarse aggregates, RCF is seldom used to replace sands in concrete due to its high surface area and attached old mortar on the surface of RCF. This study investigated potential use of RCF as microsilica sand substitute in the production of engineered cementitious composites (ECC), a unique high performance fiber-reinforced cementitious composites featuring extreme tensile strain capacity of several percent. The results showed that it is viable to use RCF as microsilica sand substitute in the production of ECC and the resulting RCF-ECCs possess decent compressive strength and strain capacity. Microstructure investigation on the component level revealed that RCF size and content modify matrix toughness and fiber/matrix interface properties. The influence of RCF size and content on ECC properties was clearly revealed and explained by the resulting fiber bridging $\sigma(\delta)$ curves of RCF-ECCs calculated from the micromechanical model. Micromechanics-

[1] Corresponding author. Tel.: +65 6790 5291; fax: +65 6791 0676. *E-mail address:* ehyang@ntu.edu.sg (E.H. Yang)

based design principle can therefore be used for ingredients selection and component tailoring of RCF-ECCs.

Keywords: Recycled concrete fines; Engineered Cementitious Composites; micromechanical model; single fiber pullout test; wedge splitting test

1. Introduction

The use of construction and demolition waste not only reduces environmental burden by minimizing landfill but also preserves the finite raw materials. Recycled concrete aggregates resulting from the demolition of old concrete structures are available currently in large quantities. Coupled with shortage of non-reactive natural aggregates, there is an urgent need to use the waste aggregates. Many studies have proven that recycled coarse aggregates (RCA) can be an excellent substitution of natural aggregates for concrete production [1-3].

Generally, it is believed that the fine fraction of recycled concrete aggregates, known as recycled concrete fines (RCF), has limited application because of its larger water absorption which can jeopardize the fresh and the hardened properties of concrete. This is attributed to the high surface area and old mortar attached to the fine particles, which creates a weak interface transition zone and prevents proper bonding between the matrix and the fines [4-6].

Investigations on the use of RCF as a partial replacement of natural sand in concrete were carried out to show that the strength at early ages was marginally lower, modulus of elasticity of concrete was reduced by 15% to 20%, and drying shrinkage of concrete was increased by about 40% [7]. A reduction of compressive strength and increased shrinkage also occurred in Khatib's work [8]. Evangelista and Brito [9] reported that the use of RCF, up to 30% replacement, did not have significant influence on the mechanical properties of concrete,

while the modulus of elasticity was reduced with the increase of RCF replacement ratio. The feasibility of utilizing RCF together with recycled coarse aggregate for self-compacting concrete has been demonstrated in [10]. The maximum compressive strength was achieved by using 25%-50% RCF as a replacement of river sand. Yaprak et al. [11] conducted experiments to prove that water absorption of RCF was higher than normal fine aggregate and air content values for the fresh concrete increased. According to the test results obtained, the compressive strength for the hardened concrete decreased.

Engineered cementitious composite (ECC) is a unique class of high performance fiber-reinforced cementitious composite (HPFRCC) developed for structural applications. ECC exhibits tensile strain-hardening behavior with strain capacity in the range of 3-5% [12], whereas the fiber content is 2% by volume or less. The ultra high ductility is achieved by optimizing the microstructure of the composite employing the micromechanics-based model [13]. This approach can take into account the fiber, matrix and interface properties on composite tensile strain-hardening behavior. Based on the design guidance of the micromechanical model, microsilica sand with average and maximum grain sizes of 110 and 200 μm respectively, is widely used. Nevertheless, the availability of microsilica sand is constrained by locality. In this research, RCF is identified as a potential candidate for substitution of microsilica sand in the production of ECC with two goals, one is to achieve high tensile ductility, and the other is to improve the sustainability of the built environment by using waste stream material [14].

2. Design guideline of RCF-ECC

2.1 Micromechanical model

ECC is designed using a well-defined micromechanical model. Desirable composite behavior can be tailored by adjusting the material microstructures. There are two fundamental requirements for strain-hardening behavior. First for all, the steady-state flat crack extension must be prevail under tension, which requires the crack tip toughness J_{tip} to be less than the complementary energy J_b' calculated from the bridging stress σ versus crack opening δ curve, as illustrated by Marshall and Cox [15].

$$J_{tip} \leq \sigma_0 \delta_0 - \int_0^{\delta_0} \sigma(\delta) d\delta = J_b' \quad (1)$$

where $J_{tip}=K_m^2/E_m$, σ_0 is the maximum bridging stress corresponding to the opening δ_0, K_m is the matrix fracture toughness, and E_m is the matrix Young's modulus. The stress-crack opening relationship $\sigma(\delta)$ was derived by using analytic tools of fracture mechanics, micromechanics, and probabilistics. As a result, the $\sigma(\delta)$ curve was expressible as a function of fiber and fiber/matrix interface properties. A numerical process was proposed by Yang et al. [16] to calculate the $\sigma(\delta)$ and to determine J_b'.

Another condition for the strain-hardening behavior is that the matrix first cracking strength σ_{fc} must not exceed the maximum fiber bridging strength σ_B.

$$\sigma_{fc} \leq \sigma_B \quad (2)$$

where σ_{fc} is determined by the matrix fracture K_m, pre-existing internal flaw size a_0, and the $\sigma(\delta)$ curve. Eqn. (1) governs the crack propagation mode, while Eqn. (2) controls the initiation of cracks. Satisfaction of both Eqns. (1) and (2) is necessary to achieve the strain-hardening behavior. Details of micromechanical model can be found in Yang and Li [13].

2.2 Use of RCF

Li et al. [17] presented results of experimental research and theoretical calculations based on micromechanics to investigate the effect of fine aggregate on the strain-hardening behavior of fiber-reinforced cementitious composites. It concluded that the addition of aggregate increases elastic modulus, matrix toughness and matrix tensile strength. A large increase in matrix toughness and matrix tensile strength can lead to a violation of the inequality sign in Eqns. (1) and (2). Therefore, to ensure a robust strain-hardening behavior in the composite, the quantity and the particle size of aggregate used in ECC have to be well selected.

The use of RCF, however, may become an advantage in ECC. The weak bonding between RCF particles and matrix may lead to lower matrix toughness and lower matrix tensile strength, which helps the composite to satisfy Eqns. (1) and (2). For that reason, larger size and higher quantity of RCF might be used to produce ECC with tensile strain-hardening behavior. In addition, the use of RCF is also desirable for economical and environmental considerations due to the substitution of microsilica sand.

3. Experimental program

3.1 Raw materials

Ordinary Portland cement (ASTM C150 Type I) was used in this study. Locally available ground granulated blast-furnace slag (GGBS) was selected as the supplementary cementitious material to partially replace cement with a constant GGBS-to-cement ratio of 0.8. The characteristics of polyvinyl alcohol (PVA) fiber are listed in Table 1. Surface of PVA fibers was coated with hydrophobic oiling agent of 1.2% by weight to control the interface properties of the fiber and matrix and 8mm short fibers were employed in synthesis of RCF-ECC. Polycarboxylate-based comb-polymer superplasticiser, ADVA® 181, was used to control rheological properties of the paste to ensure good fiber dispersion can be achieved.

Recycled concrete fines (RCF) sourced locally in Singapore. To keep the consistent grading of RCF, it was prepared according to modified Fuller's curve [18] and the resulting particle size distributions are shown as Fig. 1. Physical properties of RCF are summarized in Table 2. Due to the high water absorption of RCF, it was processed to attain saturated surface dry (SSD) state by adding water proportionally in advance.

A study of the microstructure of recycled concrete fines (RCF) showed that the particles are irregular and angular in shape and the surface is generally rough and porous. The result is consistent with that of the literature [4]. Compared with the microsilica sand, RCF particles are found to have scattered particle shapes and sizes as shown in Fig. 2, especially a lot of small grains are included in RCF sample. The RCF consists of crushed aggregate particles (Fig. 3) and partially hydrated cement paste which is made up of unhydrated cement grains and hydrated products of cement (Fig. 4).

In Fig. 3, RCF ($d < 300$ μm) showed a distinctive morphology covered by small particles, which contain calcium silicate hydrate, calcium hydroxide usually in the shape of relatively large hexagonal crystals, and ettringite of needle shape [18]. The morphological study of RCF particles reveals that: (1) the high surface area and porosity, which lead to high water absorption; (2) the coating with small particles, which damage the bond between the matrix and RCF and (3) the existence of unhydrated cement grains may contribute to self-cementing property.

3.2 Mix composition of RCF-ECC

According to the micromechanics-based design principles of ECC, RCF content and RCF particle size were identified as important factors governing the properties of RCF-ECC. An experimental program was designed to study the influence of RCF content and particle size on the matrix properties, fiber/matrix interface properties and the resulting RCF-ECC composite mechanical properties as Table 3. The first series is to evaluate the influence of particle size of RCF. The ratio of RCF to cement was fixed at a constant value of 0.2. Four groups of RCF with the maximum particle size of 2,360 μm, 1,180 μm, 600 μm, and 300 μm were used in four mixes, respectively. The second series is to understand the effect of RCF content. The maximum particle size was chosen to be 600 μm, whereas three different dosages of RCF were used in three mixes. All the ratios are by weight except the fiber content is by volume.

3.3 Testing methods

3.3.1 Composite testing

To evaluate composite performance, compressive test and bending test were performed. Three cubes (50 mm ×50 mm × 50 mm) for each mix were cast and tested in compression machine with 3,000 kN capacity under load control at a loading rate of 25 kN/min. Coupon specimens 300 mm × 75 mm × 12 mm were employed for bending test. All the specimens were cured in open air under humidity of 65% RH and temperature of 28°C conditions on average for 90 days.

3.3.2 Microstructural testing

(1) Wedge splitting test

Wedge splitting test (WST), originally introduced by Tschegg and Linsbauer in 1986 [19] and improved by Bruhwiler and Wittmann [20] is a suitable method for obtaining the fracture

energy and fracture toughness. In this research, WST method was used for the matrix toughness (same mix design as in Table 3 without the addition of fiber) based on the specimen size in [21] with its interpretation formulas as Eqns. (4)-(6) and the critical crack length procurement from cracking mouth opening displacement (CMOD) in [22] as Eqn. (3).

$$CMOD_c = \frac{P_c}{BE}\left[11.56\left(1-\frac{a_c}{D}\right)^{-2} - 9.397\right] \quad (3)$$

$$K_{ic} = (K_m) = \frac{P_c}{B\sqrt{D}}F(\propto) \quad (4)$$

$$F(\propto) = 29.6 \propto^{0.5} - 185.5 \propto^{1.5} + 665.7 \propto^{2.5} - 1017.0 \propto^{3.5} + 638.9 \propto^{4.5} \quad (5)$$

$$\alpha = \frac{a_c}{D} \quad (6)$$

where B is the thickness of the specimen, D is the depth of specimen, and a_c is the effective crack length. E is the elastic modulus of the matrix, P_c is the critical (peak) load, and $CMOD_c$ is the critical CMOD.

The loading device with specimen is displayed in Fig. 5. The loading machine used in the present study was INSTRON 5569 uniaxial testing system with the capacity of 50 kN. It was controlled by displacement with constant speed at 0.2 mm/min. The splitting force was applied onto the specimen through pulley wheels which requires being frictionless. A single central line support on the bottom of the specimen was selected to resist the vertical force component. CMOD was measured using special clip gauge with ±4 mm travel and fixed at the same height as the roller center.

Fig. 6 shows the geometry and size of the cube specimen. The initial notch that simulates the crack was made by inserting a steel plate of 1 mm thickness in the specimen during casting and taking out after one day curing. The notch depth was kept constant at 90 mm. Thereafter, all the specimens were cured in water for 90 days and dried in air one day before testing.

(2) Single fiber pullout test

Single fiber pullout tests were carried to study the influence of RCF content and particle size on fiber/matrix interface bond. The single fiber pullout test was conducted on an INSTRON 5569 uniaxial testing machine (UTM) at a speed of 0.06 mm/min. The whole setup was divided into four parts as can be seen from Fig. 7. From the bottom, an X-Y table with ±25 mm travel distance to two directions was fixed to the lower gripper of the UTM machine in order to ensure accurate fiber alignment. A 10 N load cell with 0.0001 N of accuracy was used to measure the pullout force. Samples were connected to the load cell through a T-shape sample holder with flat top surface to glue samples and a T bar to screw into the load cell. The embedded end of fiber should be avoided to glue to the sample holder since the pullout force would augment in that case. An aluminum plate, where the free end of the fiber was stuck, was clamped on the upper gripper. The free length of fiber was kept at 1 mm.

Fig. 8 shows the preparation of specimens for the single fiber pullout test. The embedment length was chosen to be around 1 mm to ensure full debonding and fiber pullout can occur. To obtain such small length, specimens were cut from thin mortar plates (20 mm × 50 mm × 5 mm) in which continuous fibers were embedded. The mortar matrix had the same mix design as in Table 3 without the addition of fibers.

Fiber/matrix interface bond can be determined from the single fiber pull-out curve. A variety of fiber pull-out models [23-25] are available to interpret the experimental data into interface bond properties. In the present research, bond properties of polyvinyl alcohol (PVA) fibers in a mortar matrix were investigated with a model described in [26], which can describe three

bond properties through the notions of the chemical bond G_d, the frictional bond τ_0 and slip hardening coefficient β.

4 Results and discussion

4.1 Compressive strength of RCF-ECC

The values of compressive strengths with varying RCF content and RCF size are showed in Table 4. Compared to the control group without RCF (RCF-0), ECC with fine RCF of 0~300 μm in Series 1 (RS-0.2-300) maintains the same level of compressive strength. This may be attributed to self-cementing properties of RCF which has been suggested in literatures [10, 27]. While the inclusion of fine RCF introduces more interface transition zones (ITZ), fine RCF may also possess higher content of unhydrated cement which improves the ITZ of the resulting RCF-ECC. Figure 9 shows the XRD results of RCFs with two particle sizes, i.e. < 300 μm and < 600 μm. As can be seen, more obvious peaks associated with compounds of CaO-SiO-AlO were detected in the finer RCF indicating more mortar existed in particles less than 300 μm. Furthermore, stronger C_2S peaks were also found in the finer particles, which suggest the presence of more unhydrated cement and potential stronger self-cementing of finer RCF particles.

When the maximum RCF size increases from 300 μm to 600 μm (RS-0.2-600), 20% compressive strength reduction is observed. Although the use of larger RCF reduces the amount of ITZ, self-cementing properties of larger RCF of 600 μm may decrease rapidly resulting in weaker ITZ and reduced compressive strength. With continuing increase of the RCF size, the compressive strength recovers to the level of above 50 MPa. This may be attributed to the greater reduction of the amount of weak ITZ and the influence of reduced self-cementing properties is not significant anymore. It should be noted that, in general, three

types of ITZ existed in concrete with recycled aggregates: the old ITZ between old mortar and natural aggregate; the new ITZ between old mortar and new cement paste; and the new ITZ between natural aggregate and the new cement paste. This is especially important for concrete with recycled coarse aggregates [28]. The recycled concrete fines; however, mainly consists of old mortar with very few natural aggregates [29, 30]. The major ITZ type in RCF-ECC of current study was believed to be the new ITZ between old mortar and new cement paste. In summary, self-cementing properties of RCF dominates the compressive strength of RCF-ECC when fine RCF is used while the amount of ITZ controls the compressive strength when larger size of RCF is used to produce RCF-ECC as shown in Fig. 10.

As for the impact of RCF content to compressive strength, the trend shows that the compressive strength reduces with increase of RCF content when RCF with maximum size of 600 μm is used. As discussed above, the contribution of RCF self-cementing diminishes rapidly with increasing RCF size and is not the dominated factor of RCF with maximum size of 600 μm. Therefore, the main cause of compressive strength reduction can be attributed to increased amount of ITZ with more RCF inclusion, which makes the composite less resistant to mechanical loads. Besides that, the porous adhered old mortar on the RCF surface can induce higher porosity, which also contributes to lower compressive strength of the composite.

4.2 Flexural behavior of RCF-ECC

Figs. 11 and 12 show the representative flexural stress versus deflection curves of Series 1 and Series 2 RCF-ECCs, respectively. As can be seen, all groups of specimens exhibit deflection-hardening with multiple cracking as shown in Fig. 13, which is the cracking state on the bottom surface of the specimen. Corresponding strain capacity of each group was

inversely calculated from the load-deflection curve according to Qian and Li [31] and was summarized in Table 4. Influence of RCF particle size on strain capacity of RCF-ECC is plotted in the same figure of compressive strength as Fig. 10. As can be seen, the effect of RCF particle size on strain capacity is the reverse of that on compressive strength. This suggests reduced matrix strength favors the formation of multiple cracking and enhances strain capacity of RCF-ECC. For series 2, both the flexural strength and strain capacity decrease with increasing RCF content. This is attributed to increased matrix toughness which is studied in detail in the following microstructural investigation.

As can be seen, inclusion of RCF may alter the performance of ECC. It is demonstrated, however, RCF-ECC can be designed to maintain their ductility provided the amount of RCF and particle size are properly controlled. To discover the underlying causes of performance difference, influence of RCF size and content on matrix and fiber/matrix interface was studied in the following section.

4.3 Influence of RCF on matrix toughness

Fig. 14 shows the typical failure mode of samples after the wedge splitting test, which breaks into two halves along the pre-notch. The test results of matrix toughness are summarized in Table 5. As can be seen, the addition of RCF both the size and the content show great influence on matrix toughness. Influence of RCF size on matrix toughness is similar to that on compressive strength, where it decreases first from 300 μm to 600 μm and increases afterwards. Based on crack trapping mechanism [32], matrix toughness increases with increased aggregate size because crack needs to make a longer detour to propagate through a larger aggregate and larger aggregate provides stronger mechanical anchoring to prevent

sliding of the fracture surfaces and to dissipate energy. The higher matrix toughness of RS-0.2-300 may be attributed to the self-cementing properties of fine RCF.

The matrix toughness of RCF-ECC increases with increased amount of RCF. Since the contribution of self-cementing is not the dominant factor for RCF with maximum size of 600 μm, increase of matrix toughness in this case is attributed to that fact that crack needs to propagate through more aggregates when more RCF is added to the matrix and therefore dissipating more energy. Similar phenomena on the influence of the inclusion of microsilica sand on matrix toughness was reported [17].

4.4 Influence of RCF on fiber/matrix interface

Table 6 summarized the fiber/matrix interface bonds obtained from the single fiber pullout test. As can be seen, chemical bond G_d decreases with increased particle size as shown in Fig. 15(a). Chemical bond describes adhesion between fiber and matrix. Higher G_d suggests stronger chemical structure between the fiber surface and the mortar matrix when smaller RCF particles are used, perhaps due to the self-cementing property of fine RCF which enhances the interface chemical adhesion. Reduced G_d generally increases the complimentary energy J_b' of fiber bridging which favors multiple cracking of ECC.

Frictional bond τ_0 first decreases with increased particle size followed by a reverse trend when large RCF is used as shown in Fig. 15(b). Frictional bond represents mechanical friction between fiber and matrix. As discussed above, the use of fine RCF (RS-0.2-300) results in higher matrix toughness due to self-cementing of fine RCF. The inclusion of coarse RCF (RS-0.2-2360) on the other can also improve toughness of the surrounding matrix as shown in Table 5 and reproduced in Fig. 15(b). Both can lead to higher mechanical friction

between fiber and matrix. The moderate frictional bond within 1~2MPa is anticipated to achieve better strain-hardening behavior due to a balanced fiber pullout and rupture behavior which maximized the complimentary energy J_b' and strength σ_B of fiber bridging [33].

Slip hardening coefficient β also decreases with increased particle size first followed by a reverse trend when large RCF is used as shown in Fig. 15(c). Slip hardening captures the phenomenon of soft polymer fiber scrapped by the surrounding hard matrix during sliding. Higher β shows that fibers are damaged more due to tougher matrix and higher interfacial friction. As mentioned, both the use of fine RCF (RS-0.2-300) or coarse RCF (RS-0.2-2360) can lead to harder matrix resulting in higher β.

With regard to the influence of RCF content as Fig.16, the general trend shows that G_d and β decrease while τ_0 slightly increases with increased RCF content. The inclusion of higher content of RCF reduces the over binder content and therefore chemical adhesion between fiber and matrix reduces as well. Higher RCF content enhances matrix toughness which can lead to higher mechanical friction.

4.5 Influence of RCF on ECC tensile strain-hardening behavior

Based on the measured interface properties in the section 4.4, influence of RCF size or content on fiber bridging σ(δ) curve and J_b' can be calculated through the numerical process proposed by Yang et al. [16]. Effects of RCF size on fiber bridging and pseudo strain-hardening (PSH) indices (J_b'/J_{tip}) are shown in Fig. 17. As can be seen, both the stiffness and the peak strength of the fiber bridging first decreases with the increase of RCF size followed by a reverse trend when large RCF is used similar to the friction bond τ_0. The complementary energy J_b', also shows a similar trend by taking into account all component properties into the

model as shown in Fig. 17(b). PSH indices were calculated based on the information obtained from Fig. 17(a) and Table 5. A PSH index beyond 1.0 indicates potential strain-hardening performance and a larger PSH index gives higher chance for saturated multiple cracking and higher strain capacity. As can be seen in Fig. 17(b), all RCF-ECCs have PSH indices larger than one and RCF-0.2-600 has the highest PSH index. This conclusion corresponds well with the measured composite performance as most of the RCF-ECCs have strain capacity above 1% (Table 4). Thereof, RS-0.2-600 exhibits the highest strain capacity of 2.03% with the formation of saturated multiple cracks.

Influence of RCF content on fiber bridging and PSH indices are shown in Fig. 18. As can be seen, the stiffness of bridging curve and peak bridging strength increase while the complementary energy J_b' decreases with the increase of RCF content due to increase of friction bond and decrease of chemical bond as shown in Fig. 16. While the PSH reduces with the increase of RCF content, all RCF-ECCs still have PSH indices larger than one. This again corresponds well with the composite performance where the strain capacity reduces with the increase of RCF content and all three RCF-ECCs have strain capacity above 1.5%. The addition of excessive RCF can lead to reduced tensile ductility with less saturated multiple cracking as shown in Table 4.

5. Conclusions

This study investigated potential use of recycled concrete fines (RCF) as microsilica sand substitute in the production of ECC. Experiments were carried out in the composite level and in the component level to reveal the influence of RCF size or content on the mechanical properties as well as matrix and fiber/matrix interface properties of the resulting RCF-ECCs.

Micromechanical model was engaged to calculate the resulting fiber bridging $\sigma(\delta)$ curves and the influence of RCF size and content on tensile strain-hardening of RCF-ECC was revealed. Inclusion of RCF may alter the performance of ECC. All RCF-ECCs produced in this study; however, still possessed decent compressive strength above 40 MPa with strain capacity more than 0.8%. It is therefore viable to use recycled concrete fines (RCF) as microsilica sand substitute in the production of ECC. Microstructure investigation on the component level revealed that RCF size and content modify matrix toughness and fiber/matrix interface properties due to various mechanisms including self-cementing of fine RCF. The fiber bridging $\sigma(\delta)$ curves as well as PSH indices can then be determined by the micromechanical model. The results clearly explained the influence of RCF size and content on ECC properties. Micromechanics-based design principle can be used for ingredients selection and component tailoring of RCF-ECCs.

Acknowledgement

This research grant is supported by the Singapore National Research Foundation under its Environmental & Water Technologies Strategic Research Programme and administered by the Environment & Water Industry Programme Office (EWI) of the PUB.

References

1. Sagoe-Crentsil KK, Brown T, and Taylor AH. Performance of concrete made with commercially produced coarse recycled concrete aggregate. Cem Concr Res 2001; 31: 707-712.

2. Katz A. Treatments for the improvement of recycled aggregate. J Mater Civ Eng, ASCE 2004; 16(6): 597-603.

3. Kou S-c, Poon C-s, and Agrela F. Comparisons of natural and recycled aggregate concretes prepared with the addition of different mineral admixtures. Cem Concr Compos 2011; 33(8): 788-795.

4. Tam VWY, Gao XF, and Tam CM. Microstructural analysis of recycled aggregate concrete produced from two-stage mixing approach. Cem Concr Res 2005; 35(6): 1195-1203.

5. Katz A and Baum H. Effect of high levels of fines content on concrete properties. ACI Mater J 2006; 103(6): 474-482.

6. Meyer C. The greening of the concrete industry. Cem Concr Compos 2009; 31(8): 601-605.

7. Ravindrarajah RS and Tam CT. Recycling concrete as fine aggregate in concrete. Int J Cem Compos Lightweight Concr 1987; 9(4): 235-241.

8. Khatib JM. Properties of concrete incorporating fine recycled aggregate. Cem Concr Res 2005; 35(4): 763-769.

9. Evangelista L and de Brito J. Mechanical behaviour of concrete made with fine recycled concrete aggregates. Cem Concr Compos 2007; 29(5): 397-401.

10. Kou SC and Poon CS. Properties of self-compacting concrete prepared with coarse and fine recycled concrete aggregates. Cem Concr Compos 2009; 31(9): 622-627.

11. Yaprak H, et al. Effects of the fine recycled concrete aggregates on the concrete properties. Int. J. Phys. Sci 2011; 6(10): 2455-2461.

12. Li VC. On Engineered Cementitious Composites (ECC)-A review of the material and its applications. J Adv Concr Technol 2003; 1(3): 215-230.

13. Yang EH and Li VC. Strain-hardening fiber cement optimization and component tailoring by means of a micromechanical model. Constr Build Mater 2010; 24(2): 130-139.

14. Lepech MD, et al. Design of green Engineered Cementitious Composites for improved sustainability. ACI Mater J 2008; 105(6): 567-575.

15. Marshall D and Cox BN. A J-integral method for calculating steady-state matrix cracking stresses in composites. Mech Mater 1988; 7: 127-133.

16. Yang EH, et al. Fiber-bridging constitutive law of Engineered Cementitious Composites. J Adv Concr Technol February 2008; 6(1): 181-193.

17. Li VC, Mishra DK, and Wu H-C. Matrix design for pseudo-strain-hardening fibre reinforced cementitious composites. Mater Struct 1995; 28: 586-595.

18. Neville AM, Properties of concrete, 4th ed. London: Addison Wesley Longman Limited, 1995

19. Linsbauer HN and Tschegg EK. Fracture energy determination of concrete with cube shaped specimens. Zement und Beton 1986; 31: 38-40.

20. Brohwiler E and Wittmann FH. The wedge spliting test, a new method of performing stable fracture mechanics tests. Eng Fract Mech 1990; 35(1/2/3): 117-125.

21. Zhao GF, Jiao H, and Xu SL. Behavior with wedge splitting test method. In: van Mier JGM, et al.,editor. Fracture process in Concrete, Rock and Ceramics. London: E & FN Spon, 1991. p. 789-798.

22. Kim YY, et al. ECC produced with granulated blast furnace slag. Available from: http://citeseerx.ist.psu.edu/viewdoc/download?doi=10.1.1.146.5213&rep=rep1&type=pdf.

23. Gao YC. Debonding along the interface of composites. Mech Res Commun 1987; 14(2): 67-72.

24. Stang H, Li Z, and Shah SP. Pullout problem stress versus fracture mechanical approach. J Eng Mech, ASCE 1990; 116(10): 2136-2150.

25. Hsueh C-H. Evaluation of interfacial shear strength, residual clamping stress and coefficient of friction for fiber-reinforced ceramic composites. Acta metall mater 1990; 38(3): 403-409.

26. Redon C, et al. Measuring and modifying interface properties of PVA fibers in ECC matrix. J Mater Civ Eng, ASCE November/December 2001: 399-406.

27. Poon CS, Qiao XC, and Chan D. The cause and influence of self-cementing properties of fine recycled concrete aggregates on the properties of unbound sub-base. Waste Manage 2006; 26: 1166-1172.

28. Li WG, Xiao JZ, Sun ZH, Kawashimab S, Shah SP. Interfacial transition zones in recycled aggregate concrete with different mixing approaches. Constr Build Mater 2012; 35: 1045-1055.

29. Poon CS, Shui ZH, and Lam L. Effect of microstructure of ITZ on compressive strength of concrete prepared with recycled aggregates. Constr Build Mater 2004; 18(6): 461-468.

30. Florea MVA and Brouwers HJH. Properties of various size fractions of crushed concrete related to process conditions and re-use. Cem Concr Res 2013; 52: 11-21.

31. Qian S and Li VC. Simplified inverse method for determining the tensile strain capacity of strain hardening cementitious composites. J Adv Concr Technol 2007; 5(2): 235-246.

32. Li VC. Crack trapping and bridging as toughening mechnisms in high strength concrete. International Conference on micromechanics of Failure of Quasi-brittle Materials. 1990. p. 579-588.

33. Li VC, et al. Interface tailoring for Strain-Hardening Polyvinyl Alcohol-Engineered Cementitious Composite(PVA-ECC). ACI Mater J 2002; 99(5): 463-472.